Polynomial chaos expansion for uncertainty quantification of dam engineering problems

Author(s):
Hariri-Ardebili, Mohammad A.; Sudret, Bruno

Publication date:
2019-01-15

Permanent link:
https://doi.org/10.3929/ethz-b-000379680

Originally published in:
Engineering Structures 203, https://doi.org/10.1016/j.engstruct.2019.109631

ETH zürich

Polynomial chaos expansion for uncertainty quantification of dam engineering problems

M.A. Hariri-Ardebili and B. Sudret

Chair of Risk, Safety and Uncertainty Quantification
Stefano-Franscini-Platz 5
CH-8093 Zürich

Risk, Safety & Uncertainty Quantification

Data Sheet

Journal:	Engineering Structures
Report Ref.:	RSUQ-2019-004
Arxiv Ref.:	https://arxiv.org/abs/1910.XXXX
DOI:	-
Date submitted:	June 13, 2019
Date accepted:	September 3, 2019

Polynomial Chaos Expansion for Uncertainty Quantification of Dam Engineering Problems

M.A. Hariri-Ardebili[1] and B. Sudret[2]

[1] *Dept. of Civil, Environmental and Architectural Engineering, University of Colorado, Boulder, USA*

[2] *Chair of Risk, Safety and Uncertainty Quantification, ETH Zurich, Switzerland*

October 4, 2019

Abstract

Uncertainty quantification is an inseparable part of risk assessment in dam engineering. Many probabilistic methods have been developed to deal with random nature of the input parameters or the system itself. In this paper, the polynomial chaos expansion (PCE) is adopted as an effective technique for uncertainty quantification of variety of dam engineering problems (specially with small data sets). Four different case studies are investigated with increasing complexities in which the static and dynamic responses are sought to predict. The limit state functions in the form of implicit and explicit are studied. Uncertainties are propagated in material properties and modeling. Depending on the problem at hand, a validation set from several thousands to couple of hundreds are used. Overall, it is found that the PCE is an effective technique to deal with uncertainty quantification in concrete dams.

Keywords: Polynomial Chaos Expansion – Probabilistic – Seismic – Epistemic Uncertainty – Uncertainty Quantification

1 Introduction

Prediction and classification is regularly used these days in dam engineering problems. Most of the efforts are concentrated on compiling and post-processing the measured data during the dam lifetime to predict the feature trend (Salazar et al., 2015). However, there are other groups which use the results of numerical simulations (e.g. finite element (FE) method) as an input to develop surrogate meta-models. Studies in this group are very limited with specific case studies. This paper will focus on the second group.

Dam engineering problems were always one of the most complex ones in the field of civil engineering (Hariri-Ardebili, 2018). Not only because of their special geometry, but also interaction of different material phases (e.g. solid-fluid), followed by large amount of material which increases the probability of heterogeneity, and finally, different nature of applied loads (e.g. thermal, dynamic, and hydrologic). Although such a coupled system requires detailed numerical procedure to solve the state equations, multiple uncertainty sources remain in the problem which should be properly quantified. Therefore, uncertainty quantification in dam engineering gained proper attention in the last decade. Most of the applications are still in the level of simulation-based approach in which a large number of FE analyses are performed to be used in reliability assessment. A large number of numerical simulations makes this technique ineffective for most of the real-world dam engineering problems.

Thus, the idea is to adopt some of the machine learning and meta-modeling techniques to reduce the computational effort while maintaining the accuracy (as much as possible). Section 1.1 provides nearly all the existing applications of soft computing in concrete dam engineering. Variety of methods such as response surface meta-model, neural network (NN), genetic algorithm, support vector machine, etc. were employed. This paper is going to explore the application of polynomial chaos expansion (PCE) in different dam engineering problems. The PCE is an effective method to replace a complex deterministic model with its meta-model (usually expressed in a simple analytical form). The probability density function (PDF) of the system's response (or quantity of interests - QoIs) can then be computed by performing a crude Monte Carlo simulation (MCS) on the meta-model.

1.1 Literature Review

This section reviews the literature on the application of machine learning and meta-modeling on concrete dams. Chen et al. (2010) implemented an improved response surface meta-model on linear dam-foundation system to evaluate the sliding probability. Karimi et al. (2010) proposed a NN model for system identification of gravity dams coupled with a hybrid boundary element-FE analysis to estimate the dynamic characteristics of the dam without reservoir. Fan et al. (2010) performed the reliability analysis by combining the response surface meta-model and finite step method to fit the explicit performance function. Then, the failure path and functionality failure mode were computed. Gu et al. (2010) proposed a least squares support vector machine procedure in the context of back analysis to identify the complex mechanical properties of dams. A complex nonlinear relationship between the relative values of hydraulic components of dam displacements and mechanical parameters is established.

Gaspar et al. (2014) proposed a probabilistic thermal model to propagate uncertainties on some RCC's physical properties where a thermo-chemo-mechanical model was used to describe the dam behavior. Cheng et al. (2015) adopted a kernel principal component analysis

to eliminate the impact of environmental variables and structural health monitoring under varying conditions. Su et al. (2016) proposed a criterion for optimal selection of back analysis parameters based on the indices from sensitivity analysis. The uniform design method was combined with a NN and support vector machine to build the mapping relationship between multiple material parameters and location-based structural responses.

Rezaiee-Pajand and Tavakoli (2015) used a combined genetic algorithm and FE for crack detection in concrete gravity dams. This method identifies the location and magnitude of cracks in dams by minimizing the difference between the analytical responses and the measured ones. Cao et al. (2017) applied fuzzy random events for stability assessment of high arch dam abutments. The associated risk ratios were proposed based on the credibility theory and calculated using the MCS and fuzzy random post-processing. Hariri-Ardebili (2018) proposed a series of design of experiments (DOEs) for reliability analysis of gravity dams. For a single problem in hand, more than 10 different DOEs were used and the accuracy and computational times were compared.

Hariri-Ardebili and Pourkamali-Anaraki (2018a,b) showed the application of several machine learning techniques in multi-hazard analysis of gravity dams. Both the simplified and the nonlinear damage models were employed. Seismic, hydrologic, and aging hazards were studied separately. They reported that machine learning techniques are useful when they are combined by FE simulations. More recently, the probabilistic response of concrete dams under hybrid uncertainties (i.e. material and modeling as epistemic and ground motion record-to-record variability as aleatory) is addressed by Hariri-Ardebili and Xu (2019); Hariri-Ardebili and Pourkamali-Anaraki (2019). The former one replaces a finite number of fractional moments by a continuous probability density function, and an improved bivariate dimension reduction method. The latter one is based on matrix completion technique to estimate the missing FE simulations using hidden information in the uncertain variables and clustering techniques.

So far, none of the above mentioned papers address the application of PCE for metamodeling of a dam engineering problem. The pioneer work belongs to Ghanem et al. (2007) where an embankment (and not concrete) dam is treated using stochastic finite element analysis, an intensive method involving PCE. The elastic and shear moduli of the material are modeled as stochastic processes with relatively low correlation length. First, the dimensionality of the problem is reduced through a Karhunen-Loève method, and then the spectral stochastic FEM including a high-dimensional polynomial in Gaussian independent variables is solved. The attained solution from coarse mesh is used to define a new basis for solving the fine mesh problem. Guo et al. (2018) are also studied stability of an embankment dam using sparse PCE. Three soil properties, including dry density, cohesion and friction angle were assumed random variables. Both the finite difference and the limit equilibrium method were used for the safety factor evaluation of the dam. The failure probability distribution under

normal exploitation conditions and seismic loading were presented. A PCE-based global sensitivity analysis was also performed to investigate the contribution of each random variable. Finally, De Falco et al. (2018) proposed a procedure for the model parameters calibration in a Bayesian context. The technique is based on replacing the initial model with a proxy one obtained through generalized PCE. It reduces the computational burden and also provides a global model error. Both a single monolith and a 3D model are studied. They used only the displacement response for the sake of simplicity.

1.2 Objectives and Structure

This paper aims to investigate the application of PCE in different aspects of design and analysis of concrete dams. To the best of the authors' knowledge (and considering a comprehensive literature survey; See Section 1.1), this is the first paper which addresses the uncertainty quantification in concrete dams in the context of PCE. The main objective of this paper is to answer the following questions: 1) How to properly employ the PCE meta-models in practical dam engineering problems?, 2) How to interpret the results from meta-modeling?, 3) How to use the PCE for uncertainty quantification?, and 4) What are the main advantages and potential limitations of the PCE in dam engineering applications?

To properly respond to these questions, four different case studies are discussed, which covers a wide range of dam engineering problems. The novelties of this paper rely on developing several frameworks for the application of PCE in: 1) problems with implicit or explicit limit state (LS) functions, 2) simplified analytical models *vs.* advanced FE analyses, 3) static *vs.* dynamic simulations, 4) problems with discrete *vs.* continuous responses, 5) 2D *vs.* 3D problems, and finally, 6) the vibrational response of dams and heath monitoring. These features cover nearly all the aspects in material and modeling uncertainty; however, the ground motion record-to-record variability (Hariri-Ardebili and Saouma, 2016), and macro-level concrete heterogeneity (Hariri-Ardebili et al., 2019) are not discussed in this paper (due to page limit).

A brief review of PCE is provided in Section 2 for those readers who are less familiar with this concept. The detailed description of four case studies including material and loading is then given in Section 3. Finally, the results are discussed in Section 4, and the conclusions in Section 5.

2 Polynomial Chaos Expansions

2.1 Constructing the Polynomial Basis

Let us consider a system in which its computational model can be represented by $\mathcal{M}$ and is a function of M input parameters. Due to uncertainty, there parameters are modeled by a M dimensional $\boldsymbol{X} = \{X_1, X_2, ..., X_M\}$. The components are assumed to be statistically

independent, with marginal probability density functions $f_{X_i}, i = 1, ..., M$. The resulting joint distribution is denoted by $f_{\boldsymbol{X}}$. Thus, the scalar QoI resulted from this system is also a random variable, denoted $Y = \mathcal{M}(\boldsymbol{X})$. Knowing that the response random variable Y has a finite variance, $\mathbb{E}\left[Y^2\right] < \infty$, it can be represented as a PCE (Ghanem and Spanos, 2003):

$$Y = \sum_{\boldsymbol{\alpha} \in \mathbb{N}^M} y_{\boldsymbol{\alpha}} \Psi_{\boldsymbol{\alpha}}(\boldsymbol{X}) \tag{1}$$

where $\Psi_{\boldsymbol{\alpha}}(\boldsymbol{X})$ are the multi-variate polynomials orthonormal with respect to $f_{\boldsymbol{X}}$, $y_{\boldsymbol{\alpha}} \in \mathbb{R}$ are the expansion coefficients to be determined, and $\boldsymbol{\alpha} \in \mathbb{N}^M$ are multi-indices that identify the components of the multi-variate polynomials.

The multi-variate polynomials are assembled as the tensor product of their univariate counterparts (Sudret, 2008):

$$\Psi_{\boldsymbol{\alpha}}(\mathbf{x}) = \prod_{i=1}^{M} \phi_{\alpha_i}^{(i)}(x_i) \tag{2}$$

where $\phi_{\alpha_i}^{(i)}$ is the univariate orthogonal polynomial in the i^{th} variable of degree α_i where orthogonality is meant with respect to the probability density function f_{X_i} of this ith variable. A list of commonly-used classical univariate polynomial families can be found in Xiu and Karniadakis (2002). To be used in the context of real-world problems, the summation in Equation 1 should be limited to a finite sum:

$$Y^{PCE} = \mathcal{M}^{PCE}(\boldsymbol{X}) = \sum_{\boldsymbol{\alpha} \in \mathcal{A}} y_{\boldsymbol{\alpha}} \Psi_{\boldsymbol{\alpha}}(\boldsymbol{X}) \tag{3}$$

where $\mathcal{A}$ is the truncation set of multi-indices of cardinality P. There are two main truncation schemes, i.e. standard (Fajraoui et al., 2017) and hyperbolic (Blatman and Sudret, 2011). The former one is based on selecting all polynomials in M input random variables of total degree not exceeding p:

$$\mathcal{A}^{M,p} = \left\{\boldsymbol{\alpha} \in \mathbb{N}^M \ : \ |\boldsymbol{\alpha}| \leq p\right\} \qquad \operatorname{card} \mathcal{A}^{M,p} \equiv P = \binom{M+p}{p} = \frac{(M+p)!}{p!\ M!} \tag{4}$$

The hyperbolic truncation is, in fact, a modification to the standard version, and uses the parametric q-norm to define the truncation:

$$\mathcal{A}^{M,p,q} = \left\{\boldsymbol{\alpha} \in \mathcal{A}^{M,p} \ : \ \|\boldsymbol{\alpha}\|_q \leq p\right\}, \qquad \|\boldsymbol{\alpha}\|_q = \left(\sum_{i=1}^{M} \alpha_i^q\right)^{1/q} \tag{5}$$

For q=1, the hyperbolic truncation corresponds to the standard one. For $q < 1$, hyperbolic truncation includes all univariate polynomials up to degree p, yet for less polynomials that depend on many parameters. Figure 1 illustrates a set of 2D hyperbolic truncation with varying p and q. As seen, decreasing the value of q decreases the number of mixed order polynomials in the expansion.

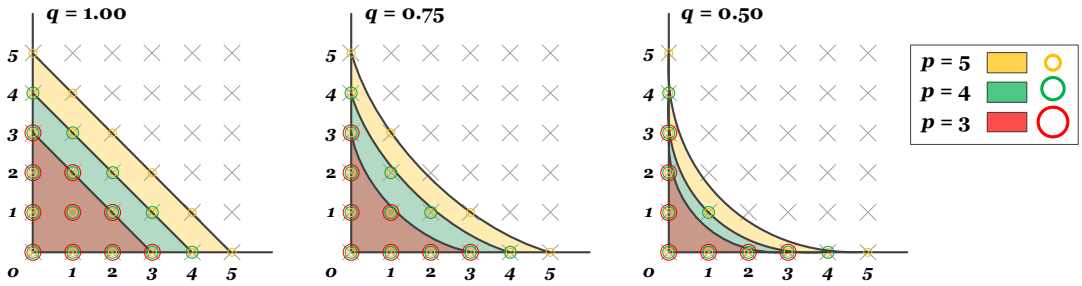

Figure 1: Illustration of the hyperbolic truncation set with varying p (3 to 5) and q (0.5 to 1.0)

2.2 Computing the Expansion Coefficients

The expansion coefficients might be computed either using intrusive or non-intrusive approaches. The former one is originally proposed in the context of the stochastic finite element method (Ghanem and Spanos, 1991) to discretize the constitutive equations both in the physical and the random spaces. The latter one relies on post-processing of the outputs from multiple simulations, so-called DOE (Cavazzuti, 2012), of the existing numerical model. There are multiple strategies to compute the expansion coefficients non-intrusively, among them the least-square minimization is well-established (Berveiller et al., 2006). Least-squares minimization adapts the candidate polynomial basis one after the other and computes the corresponding PCE. The least angle regression (LAR) leads to sparse PCE, where polynomials are selected from a candidate truncation scheme, only the polynomials that have the largest impact on the model response are retained (while the other coefficients are set to zero).

Based on Equations 1 and 3, one can write the infinite series as a sum of its truncated set and a residual:

$$\mathcal{M}(\boldsymbol{X}) = \mathcal{M}^{PCE}(\boldsymbol{X}) + \varepsilon_P = \sum_{j=0}^{P-1} y_i \Psi_j(\boldsymbol{X}) \equiv \boldsymbol{y}^T \Psi(\boldsymbol{X}) + \varepsilon_P \tag{6}$$

where ε_P is the truncation error, and superscript T means transpose.

The LAR method consists in finding a set of coefficients $\boldsymbol{y}$ which minimizes the mean square error including a penalty term of the form $\lambda \|\boldsymbol{y}\|_1$ as (Efron et al., 2004):

$$\hat{\boldsymbol{y}} = \underset{\boldsymbol{y} \in \mathbb{R}^P}{\arg\min}\, \mathbb{E}\left[\left(\boldsymbol{y}^T \Psi(\mathbf{X}) - \mathcal{M}(\mathbf{X})\right)^2\right] + \lambda \|\boldsymbol{y}\|_1 \tag{7}$$

where $\|\hat{\boldsymbol{y}}\|_1 = \sum_{\boldsymbol{\alpha} \in \boldsymbol{A}} |y_\alpha|$ is the regularization term that forces the minimization to favor sparse solutions. The LAR algorithm can be summarized in the following iterative procedure (Blatman and Sudret, 2011):

1. Initialization the parameters: $y_{\boldsymbol{\alpha}} = 0$; $\forall \boldsymbol{\alpha} \in \boldsymbol{A}$; candidate set of $\Psi_{\boldsymbol{\alpha}}$, active set of $\emptyset$, and set the residuals equal to the vector of observations $\boldsymbol{y}$.
2. Find the vector $\Psi_{\boldsymbol{\alpha}_j}$ which is most correlated with the current residual.

3. Move $y_{\boldsymbol{\alpha}}$ from zero towards their least-square value until their regressors $\Psi_{\boldsymbol{\alpha}_j}$ are equally correlated to the residual as some other regressor in the candidate set.
4. Compute the so-called leave-one-out error, Err^j_{LOO} for the current iteration (will be explained later), update all the active coefficients, and move $\Psi_{\boldsymbol{\alpha}_j}$ from candidate set to the active set.
5. Continue this step until the size of the active step becomes $\min(N-1, P)$.

The residual error, ε_P, in Equation 6 can be further computed using two techniques (Marelli and Sudret, 2015):

- Normalized empirical error (NEE) is an estimator of the generalized error based on the response of meta-model to the DOE points:

$$Err_{\text{NEE}} = \frac{\sum_{i=1}^{N} \left(\mathcal{M}\left(\boldsymbol{x}^{(i)}\right) - \mathcal{M}^{PCE}\left(\boldsymbol{x}^{(i)}\right)\right)^2}{\sum_{i=1}^{N} \left(\mathcal{M}\left(\boldsymbol{x}^{(i)}\right) - \frac{1}{N}\sum_{i=1}^{N} \mathcal{M}\left(\boldsymbol{x}^{(i)}\right)\right)^2} \tag{8}$$

- Leave-one-out (LOO) cross validation technique is intended to overcome the over-fitting limitation of NEE using cross validation technique. First, a single DOE point is left out at a time, and then, a polynomial chaos expansion $\mathcal{M}^{PCE\setminus i}$ is constructed using the remaining points (Blatman and Sudret, 2010). Subsequently, the error is computed as follows after some algebra simplifications:

$$Err_{\text{LOO}} = \frac{\sum_{i=1}^{N} \left(\frac{\mathcal{M}\left(\boldsymbol{x}^{(i)}\right) - \mathcal{M}^{PCE}\left(\boldsymbol{x}^{(i)}\right)}{1 - \text{diag}\left(\boldsymbol{A}(\boldsymbol{A}^T\boldsymbol{A})^{-1}\boldsymbol{A}^T\right)}\right)^2}{\sum_{i=1}^{N} \left(\mathcal{M}\left(\boldsymbol{x}^{(i)}\right) - \frac{1}{N}\sum_{i=1}^{N} \mathcal{M}\left(\boldsymbol{x}^{(i)}\right)\right)^2} \tag{9}$$

  where $\boldsymbol{A}$ is the information matrix of size $N \times P$, which contains evaluations of all base polynomials at all points of the DOE, namely $A_{ij} = \Psi_j(\boldsymbol{x}^{(i)})$.

Over-fitting is a concept that stems from machine/statistical learning. When a model (e.g., NN, PCE, etc.) is built to approximate an input/output relationship from data (either a given data set in the usual machine learning setting, or the experimental designed selected by the analyst in the context of PCE), there must be a trade-off between the number of data points and the "complexity" of the fitted model. The latter can be seen as the number of parameters to compute (in our case, the number of PCE coefficients), which depends on the highest polynomial degree. If one tries to fit a large number of coefficients with a limited number of data points, one obtains a model that has little error on the data points used for its construction (possibly zero, think about an interpolating Lagrange polynomial), while it can have large errors for new input points. In other words, the model is over-fitted on the data points and has no predictive capabilities for other points.

One classical way to avoid this in machine learning (e.g., NN) is to split the data into a training and a validation sets: the model is fitted using only the points in the training

set and the error is judged on the validation set. In the case of surrogate modeling and in particular PCE, one is interested in small data sets (i.e., small experimental designs) and it is of interest to avoid setting apart validation points. This is achieved by so-called LOO cross validation, Equation 9. More details can be found in Friedman et al. (2001).

3 Application in Dam Engineering Problems

Four examples of concrete dams with different complexities are explained in this section. They are: 1) analytical model of a gravity dam, 2) simplified finite element analysis of a gravity dam, 3) detailed coupled analysis of an arch dam-foundation-reservoir system, and 4) frequency analysis of an arch dam with stage construction. Each of these problems includes different features and complexities and seek different QoIs related to the concrete dam safety assessment. Figure 2 summarizes all these problems with a representative plot including the loading and sample results.

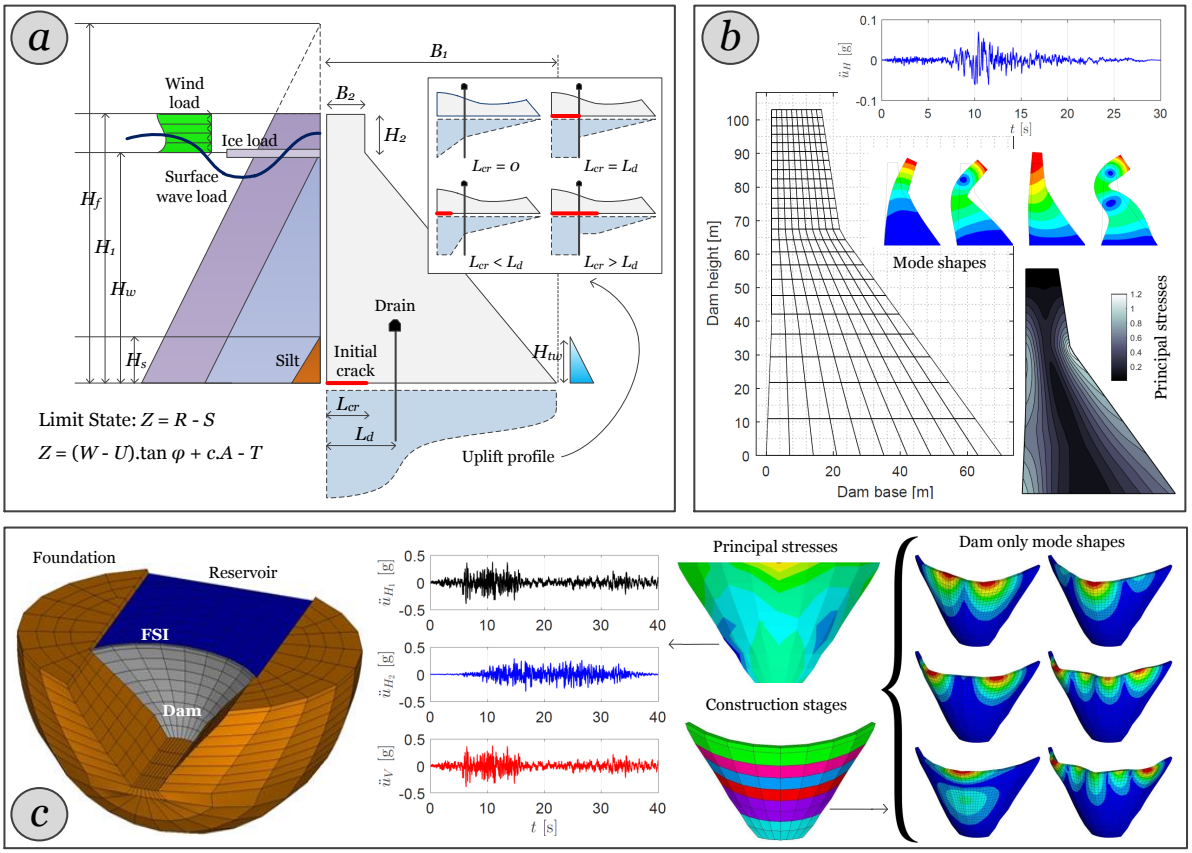

Figure 2: Model description of four case studies in this paper including geometry, loads, and sample QoIs; (a) analytical gravity dam; (b) 2D simplified finite element gravity dam model for seismic analysis; (c) 3D reservoir-foundation-arch-dam for both seismic analysis and free vibration

3.1 Analytical Gravity Dam Model

This case study is, in fact, a classical reliability analysis of a gravity dam based on limit equilibrium method. In this technique, the dam is assumed to be a rigid body and the loads are applied statically. Internal stresses are not computed, and only the magnitude and the moment arm of the resultant loads are important. The applied loads are: 1) self-weight W, 2) static uplift pressure U, 3) hydrostatic (based on normal or flood water levels) pressure P_{hyd}, 4) silt pressure P_{silt}, 5) ice pressure P_{ice}, 6) wind load P_{wind}, and 7) surface wave load P_{wave}. The uplift pressure is updated (as a function $g(.)$) based on the crack length L_{cr}, drain location L_d, the head water, H_w, and tail water, H_{tw}, pressures. Figure 2 (a) illustrates all the effective loads as well as the dam dimensions.

In this showcase, the LS function is presented explicitly and the material properties and the static loads are all assumed to be random variables. Table 1 presents the parameters considered in this analytical model and their probability density functions. All the random variables in this table (and also Tables 2 and 3) have physical meaning. Therefore, they can not exceed a certain threshold for any practical problem. The last column provides potential lower and upper bound limits for each random variable (which are based on either literature review or engineering judgment). Although different LS functions can be defined for the sliding and overturning of the dam, a global LS is used in this example which accounts for the sliding at the dam-foundation interface as:

$$Z = R - S = \left(W - \underbrace{g\left(L_{cr}, L_d, H_w, H_{tw}\right)}_{U} \right) . \tan\varphi + c.A - \underbrace{\left(P_{hyd}+P_{silt}+P_{ice}+P_{wind}+P_{wave}\right)}_{T} \tag{10}$$

where R and S are average resistance (i.e., capacity) and stress (i.e., applied load or demand), T is shear force, φ and c are angle of friction and cohesion respectively, and A_{eff} is the effective area of rupture.

The LS function is programmed in MATLAB (2016). If capacity exceeds demand, $Z > 0$, the system is in a safe state. If demand exceeds capacity, $Z < 0$, the system is in a failure state.

3.2 Simplified Gravity Dam Finite Element Model

This second example deals with simplified seismic analysis of a gravity dam. Koyna Dam is used as case study. Its height is 103.0 m, and the thickness at the base and the crest are 70.2 m and 14.8 m, respectively for the central non-overflow monoliths. Figure 2 (b) shows the cross section of the dam including a relatively coarse mesh. The finite element code EAGD (Fenves and Chopra, 1984) is used to perform dynamic analyses.

In the simplified finite element method, three different sub-structures are used for the dam, water and foundation. They are idealized independently, and are only coupled through

Table 1: Parameters considered for the analytical LS function example based on limit equilibrium method; adopted from (Hariri-Ardebili and Pourkamali-Anaraki, 2018b)

Parameter	Symbol	Unit	Model	Quantity	Bound
Width at the base	B_1	m	-	70.0	-
Width at the crest	B_2	m	-	5.6	-
Height of the dam	H_1	m	-	100.0	-
Height of the neck	H_2	m	-	6.0	-
Location of drainage	L_d	m	-	10.5	-
Pre-existing crack at the base	L_{cr}	m	Uniform	U(0.0, 28.0)	-
Pre-existing crack at the neck	L_{cr}^n	m	Uniform	U(0.0, 1.0)	-
Height of the water	H_w	m	Lognormal	LN(82.8, 22.1)	(40.0, 120.0)
Height of the silt layer	H_s	m	Normal	N(10.0, 6.0)	(1.0, 30.0)
Height of the surface wave	H_{sw}	m	Normal	N(1.0, 0.5)	(0.1, 2.0)
Concrete mass density	ρ_c	kg/m^3	Normal	N(2400, 100)	(2200, 2600)
Water mass density	ρ_w	kg/m^3	-	1000	-
Silt mass density	ρ_s	kg/m^3	Normal	N(1850, 50)	(1750, 2000)
Rock-concrete cohesion	c_{rc}	MPa	Lognormal	LN(0.62, 0.17)	(0.2, 2.0)
Rock-concrete friction angle	ϕ_{rc}	deg.	Normal	N(30.0, 7.0)	(15.0, 45.0)
Concrete-concrete cohesion	c_{cc}	MPa	Lognormal	LN(0.71, 0.13)	(0.5, 2.0)
Concrete-concrete friction angle	ϕ_{cc}	deg.	Normal	N(34.0, 6.0)	(20.0, 45.0)
Drain efficiency	eff_D	-	Uniform	U(0.01, 0.99)	-
Silt internal friction angle	ϕ_s	deg.	Normal	N(30.0, 8.0)	(15.0, 45.0)
Wind pressure	P_{wind}	Pa	Uniform	U(100, 150)	-
Ice pressure	P_{ice}	Pa	Normal	N(300, 150)	(100, 1500)
Ice thickness	t_{ice}	m	Normal	N(0.4, 0.3)	(0.01, 1.0)

the interaction forces and appropriate compatibility conditions. In this simplified method, the coupled equations of motion are written in frequency domain. While the dam is modeled as a 2D finite element system, the water is idealized by a fluid domain of constant depth and infinite length. The foundation rock is also idealized as a homogeneous, isotropic, viscoelastic half-plane. The dam-foundation interaction effects are included by adding the dynamic stiffness matrix for the rock region in the equations of motion. The stiffness matrix is frequency-dependent, and is defined with respect to the degree of freedom of the nodal points at the dam base.

In this case study, the applied loads are: dam self-weight, hydrostatic pressure (reservoir is assumed 89% filled), bottom sediment (wave reflection coefficient for the reservoir bottom materials is assumed to be 0.75), and the (horizontal component of) ground motion excitation (Loma Prieta earthquake of 1989 at San Francisco 1295 Shafter station with 6.9 magnitude). Note that this is a relatively low intensity excitation (representative for majority of the recorded motions in PEER (2017)) to keep the dam (stress) response in linear domain. The free-field ground acceleration is applied to the system and it is assumed to be identical at all points on the base of the dam. Figure 2 (b) also shows the envelope of maximum first principal stresses within the dam body (for the reference model), as well as the four vibrational modes.

In this example, the material properties and the vibration characteristics for the concrete and rock are assumed to be uncertain, see the properties of the random variables in Table 2. Monte Carlo simulation is performed using Latin Hypercube Sampling (LHS) (McKay et al.,

1979; Olsson and Sandberg, 2002) with N_{sim} = 1,000 dynamic analyses. No correlation is assumed among the random variables. QoIs are extracted in terms of the displacement and principal stresses. The results of these 1,000 simulations are later used in PCE meta-models. Note that in this example, only the epistemic uncertainty is investigated (since it is due to limited data and knowledge), and the seismic load (i.e., aleatory uncertainty) is assumed unchanged for all the simulations.

Table 2: Material properties for the gravity dam; adopted from (Hariri-Ardebili and Boodagh, 2018)

Quantity	Symbol	Unit	Model	Quantity	Bound
Concrete modulus of elasticity	E_c	MPa	Normal	$N(23,950, 2,395)$	(19,100 28,800)
Concrete Poisson's ratio	ν_c	-	-	0.2	-
Concrete mass density	ρ_c	kg/m^3	Normal	$N(2,470, 247)$	(2,160 2,790)
Concrete hysteretic damping	η_c	-	Normal	$N(0.06, 0.02)$	(0.02 0.10)
Foundation modulus of elasticity	E_f	MPa	Normal	$N(21,550, 2,155)$	(17,700 25,400)
Foundation Poisson's ratio	ν_f	-	-	0.33	-
Foundation mass density	ρ_f	kg/m^3	Normal	$N(2,680, 268)$	(2,320 3,040)
Foundation hysteretic damping	η_f	-	Normal	$N(0.05, 0.02)$	(0.02 0.08)

3.3 Coupled Arch Dam-Reservoir-Foundation Model

Two previous examples included 2D analysis of gravity dams. This third example addresses the seismic analysis of a 3D arch dam-reservoir-foundation coupled system. Karaj Dam is selected as the case study. This dam offers a symmetric double curvature; its crest is 390.0 m long and it extends a height of 168.0 m above the foundation. The dam structure and foundation medium have been modeled using 20-node isoparametric elements. The radius of the foundation region, which was modeled in a semi-spherical shape, was set at 330 m, with the center of the semi-spherical body located at the middle of the dam body crest. The foundation is assumed to be massless. The reservoir was simulated using 8-node isoparametric fluid elements extending roughly twice the dam height in the upstream direction.

Fluid-structure interaction is modeled based on Eulerian-Lagrangian approach. In this technique, the unknown variables are the displacements (in the solid domain) and the pressures (in the fluid domain). It is assumed that the water is linearly compressible and its viscosity is neglected (Liaw and Chopra, 1974; Bouaanani and Lu, 2009). The coupled system boundary conditions are summarized in Equation 11, and are solved using a staggered solution.

$$\begin{cases} \bigtriangledown^2 P(x,y,z) = \frac{1}{c_0^2}\ddot{P}(x,y,z,t) & \text{Pressure wave equation} \\ \frac{\partial P(x,y,z,t)}{\partial n} = -\rho_w a_n^s(x,y,z,t) & \text{Dam-reservoir interface} \\ \frac{\partial P(0,t)}{\partial n} = -\rho_w a_n(t) + \frac{(1-\alpha_w)}{c_0(1+\alpha_w)}\frac{\partial P(0,t)}{\partial t} & \text{Foundation-reservoir interface} \\ \frac{\partial P}{\partial n} = -\frac{1}{c_0}\frac{\partial P}{\partial t} & \text{Reservoir far-end boundary} \\ P(x,y,z,t) = 0 & \text{Reservoir free surface} \end{cases} \quad (11)$$

where P is the hydrodynamic pressure, c_0 the pressure wave velocity in water, ρ_w water density, a_n normal acceleration, s represents the dam face, and α_w is the wave reflection coefficient at the reservoir bottom and sides.

The finite element model of the dam-reservoir-foundation system is shown in Figure 2 (c). Only three material properties are assumed to be uncertain, see Table 3, and the coupled system is excited using a three component ground motion record. Manjil ground motion recorded at the Abbar station during Manjil-Iran earthquake on 20 June 1990 was used frequently to analyze this dam (Mirzabozorg et al., 2010). The mass and stiffness proportional damping is applied on the structure whose damping ratio for the fundamental mode has been selected to be 5%. The pressure wave propagation velocity and density of water equal 1,436 m/s and 1,000 kg/m^3, respectively. Since the problem at hand is linear elastic, none of the vertical joints are modeled. Also, the damage response of mass concrete is neglected. This is to simplify the model for probabilistic simulations. A detailed nonlinear analysis of arch dam with nearly all nonlinearity and interaction sources can be found in Hariri-Ardebili and Kianoush (2014).

Multiple transient analyses are performed on the coupled system with different sample sizes and techniques. QoIs are extracted in term of displacement time histories and principals stresses.

Table 3: Material properties for the arch dam (Hariri-Ardebili and Kianoush, 2014)

Quantity	Symbol	Unit	Model	Quantity	Bound
Concrete modulus of elasticity	E_c	MPa	Normal	$N(30,000, 4,500)$	(20,000 40,000)
Concrete Poisson's ratio	ν_c	-	-	0.17	-
Concrete mass density	ρ_c	kg/m^3	Normal	$N(2,400, 120)$	(2,150 2,600)
Foundation modulus of elasticity	E_f	MPa	Normal	$N(30,000, 6,000)$	(20,000 40,000)
Foundation Poisson's ratio	ν_f	-	-	0.15	-

3.4 Layered Arch Dams Vibration Characteristics

The final case study deals with frequency analysis of the previous arch dam. As oppose to the third example, the concrete is not considered homogeneous anymore, and different values of moduli of elasticity is assumed for various layers. The source of this material variation can be attributed to: 1) staged construction process of arch dams in which different concrete batches might be used with different cement and aggregate sources, mixing process, and the in-situ vibration process; and/or 2) different degradation rate (e.g., alkali aggregate reaction) for different zones as a combination of non-homogeneous temperature and moisture distribution (Saouma, V., 2014).

Overall, six stages of construction are assumed and the random modulus of elasticity is assigned based on a uniform distribution in the range of (17.5, 32.5) GPa. All the other material properties are kept constant. QoIs are extracted in the form of vibration frequencies, participation factors and effective masses in six (translational and rotational) directions, and

the mode shapes. The dam with varying layers, as well as several sample mode shapes are shown in Figure 2 (c).

4 Results

This section presents the detailed results of the PCE-based uncertainty quantification on the dam engineering problems with different complexities. According to the general framework of uncertainty quantification introduced by Sudret (2007), for every type of uncertainty analysis up to three ingredients can be identified, See Figure 3:

- Step A: A computational model (in this paper different dam engineering problems) used to compute several QoIs to the analyst. This model is (in majority of cases) a black-box map of the form $Y = \mathcal{M}(\boldsymbol{X})$ that, provides a set of responses Y for every combination of input parameters $\boldsymbol{X}$.
- Step B: A model of the uncertainty in the input parameters, $\boldsymbol{X}$, due to aleatory and/or epistemic nature of variability. It is usually presented in the form of probabilistic models.
- Step C: An uncertainty analysis that aims at combining the epistemic/aleatory uncertainties with the computational model, to quantify some property in the stochastic system (e.g., mean, variance). The PCE meta-model, $\mathcal{M}^{PCE}$, is used as a tool for uncertainty analysis in this paper.

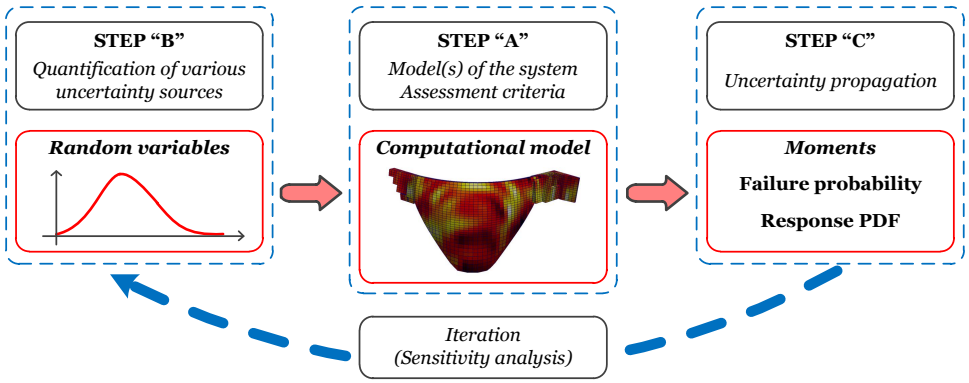

Figure 3: The general uncertainty quantification framework; adopted from (Marelli and Sudret, 2014)

The overall goal in this section is to answer two important questions: 1) Can the PCE meta-model be used for uncertainty quantification of dam engineering problems?; if yes, 2) How much computational time/cost is saved through employing the PCE method?

The answer for the first question will be achieved by comparing the PCE estimated QoIs with those obtained from analytical/FE methods. On the other hand, the computational cost is directly estimated by the minimum number of simulations that the PCE method needs to

build a surrogate meta-model with a desired accuracy. It means that efficiency of the PCE is evaluated as $\frac{N_{DOE}}{N_{sim}}$. In the following sections, the number of initial simulations, N_{sim}, used in conventional probabilistic analyses is first provided. Next, different PCE meta-models are built using fraction of the initial simulations, N_{DOE}. Although it is intuitive that more N_{DOE} yields to a better meta-model, the optimal value is introduced for the problems in hand. These values can be used as a guide for similar cases.

In all the examples (case studies), generalized PCEs are used in the software UQLab (Marelli and Sudret, 2014), i.e., orthogonal polynomials are selected for each variable according to the corresponding input distribution. For standard distributions, analytical polynomials from the Wiener-Askey scheme are used (e.g., Legendre for uniform variables, Hermite for Gaussian variables) (Xiu and Karniadakis, 2002). When truncated distributions are used, the related orthogonal polynomials are computed numerically using the Stieltjes procedure. Multivariate polynomials are obtained by tensor product. All the calculations have been carried out with the open-source software UQLab, which allows for easy reproducibility. All the finite element models are also available upon the request.

4.1 Analytical Gravity Dam Model

This section presents the results of PCE on the analytical model with explicit LS function. According to Equation 10, the LS might take the positive (safe) and negative (failed) values. Although a simple case study, this method is usually used for preliminary assessment of geo-structures. Using more than ten random variables in Table 1, 1,000 simulations are generated based on LHS method and used as reference.

First, a sensitivity analysis is performed based on both traditional methods (i.e. linear input/output correlation and standard regression analysis) and the Sobol indices, Figure 4. All these methods give remarkably consistent results. This shows that the most influencing parameters are base crack length, head water level, cohesion and friction angle at the base, and drain efficiency.

PCE models are developed based on LAR method with q set to 0.75 (Equation 5). Please note that all the random variables are used in the meta-modeling regardless of their importance in sensitivity analysis. Different DOEs (with 50 to 400 points) are used to evaluate the sensitivity and accuracy of the prediction. Figure 5 shows a sample prediction (in the first row) and corresponding expansion coefficients (the second row). Four initial (and deterministic) DOE values are considered, i.e. 50, 100, 200 and 400. Obviously, increasing the initial sample size, increases the accuracy of PCE model. Also it increases the number of expansion coefficients required for the meta-modeling.

In Figures 5(a) to 5(c) (and in general, in all the similar plots in this paper), the estimated QoIs is shown in vertical axis, Y^{PCE}, while the analytical (or FEM) results are in horizontal axis, $Y^{Analytical}$ (or Y^{FEM}). In this first example, Y equals to Z (Equation

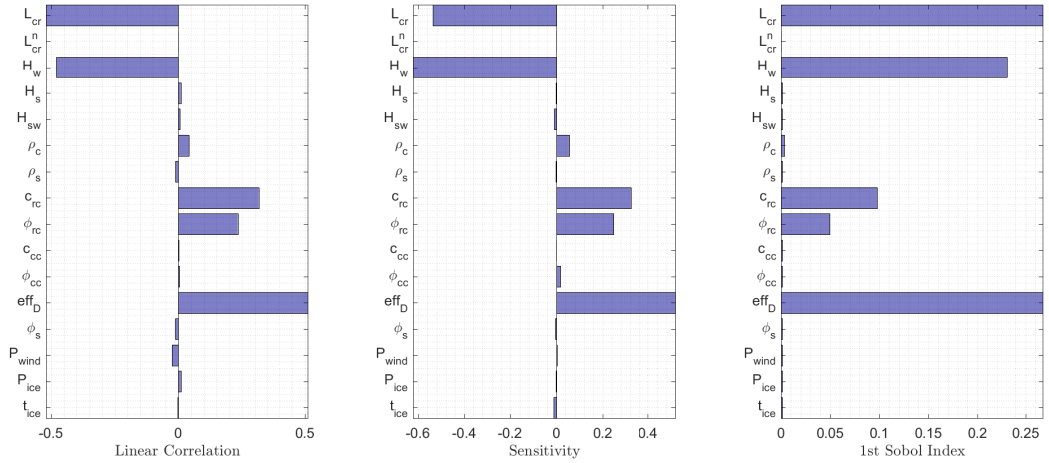

(a) Linear input/output correlation (b) Standard regression correlation (c) Sobol indices

Figure 4: Example 1; Sensitivity analysis

10). In Figures 5(e) to 5(g), the expansion coefficients, y_α, are shown in a logarithmic form. Since the coefficients might be positive or negative, a "black dot" (inside the circle) is used to distinguish the positive ones. Results are also categorized by color and size for different degrees, p. All the degrees up to three are shown separately, while the higher order ones are collected under $p > 3$. Note that not all the α have value. For example, there are only 16 coefficients in Figure 5(e).

The moments of the PCE meta-models are encoded in its coefficients because of the orthonormality of the polynomial basis. The mean and variance of a PCE can be computed as:

$$\mu^{PCE} = \mathbb{E}\left[\mathcal{M}^{PCE}(\boldsymbol{X})\right] = y_0 \; ; \qquad Var^{PCE} = \mathbb{E}\left[\left(\mathcal{M}^{PCE}(\boldsymbol{X}) - \mu^{PCE}\right)^2\right] = \sum_{\boldsymbol{\alpha}\in\mathcal{A},\boldsymbol{\alpha}\neq 0} y_{\boldsymbol{\alpha}}^2 \tag{12}$$

where y_0 is the coefficient of the constant basis Ψ_1, and variance is the summation of all the square of the coefficients for non-constant basis elements.

Since deterministic DOE values, used in Figure 5, cannot quantify the uncertainty in meta-modeling (due to the random sampling of the experimental design), a probabilistic version (with 100 replications) is presented in Figure 6. This figure, in fact, summarizes the mean and standard deviation (STD) of different metrics related to the meta-model as a function of N_{DOE}. The following observations can be drawn:

- Mean value is stable after $N_{DOE} = 100$, Figure 6(a). There is a large STD for the meta-models with $N_{DOE} = 50$.
- Variance of the meta-model output is increased by increasing the N_{DOE}, but its STD yields to a small value, Figure 6(b).

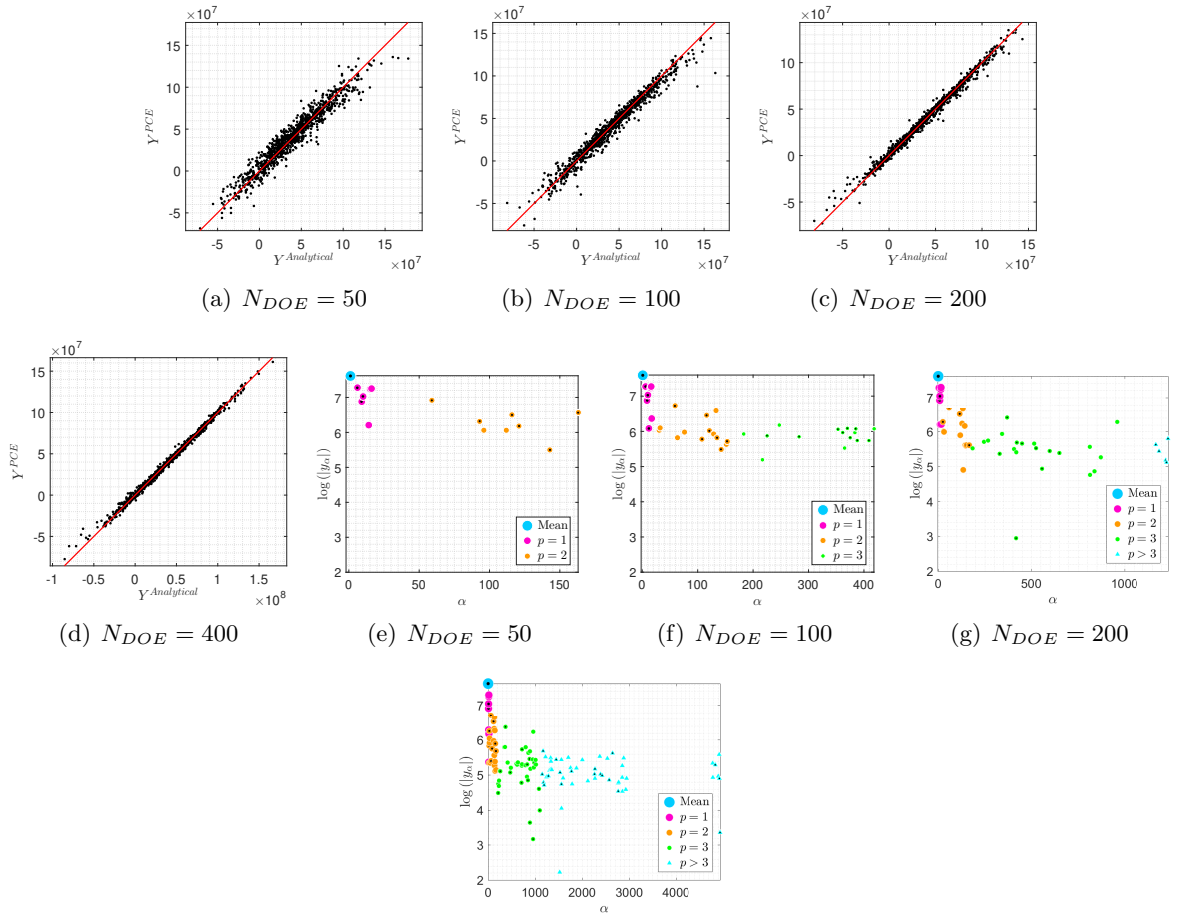

(a) $N_{DOE} = 50$ (b) $N_{DOE} = 100$ (c) $N_{DOE} = 200$

(d) $N_{DOE} = 400$ (e) $N_{DOE} = 50$ (f) $N_{DOE} = 100$ (g) $N_{DOE} = 200$

(h) $N_{DOE} = 400$

Figure 5: Example 1; PCE meta-model; LAR technique; Reference model $N_{LHS} = 1000$; N_{DOE} is variable; meta-modeling is based on Z

- The mean and STD of the number of non-zero coefficients is also increased by N_{DOE}, Figure 6(c). In average, a meta-model based on 200 DOE points has three times more expansion coefficients than the one based on 50 DOE points.
- Both the LOO and NEE residual errors decrease with increasing N_{DOE}, Figures 6(d) and 6(e). STD of the meta-model predictions with N_{DOE} equal or greater than 200 is practically zero. This means that the obtained results do not depend anymore on the sampling of the DOE when its size is greater than 200.

Results are further expanded from a reliability point of view. For the analytical problem in Example 1, it is possible to use some of the classical structural reliability analysis techniques (e.g. first-order reliability (FORM), second-order reliability method (SORM)) to obtain the failure probability, P_f, under the current load condition. First, a crude MCS with 1,000,000 simulations is performed to find a stable P_f for the problem, Figure 7(a). This plot also presents the confidence intervals. According to crude MCS, P_f is equal to 0.1333. FORM and SORM provide a failure probability of 0.1596 (∼20% overestimation) and 0.1149 (∼14% underestimation), respectively.

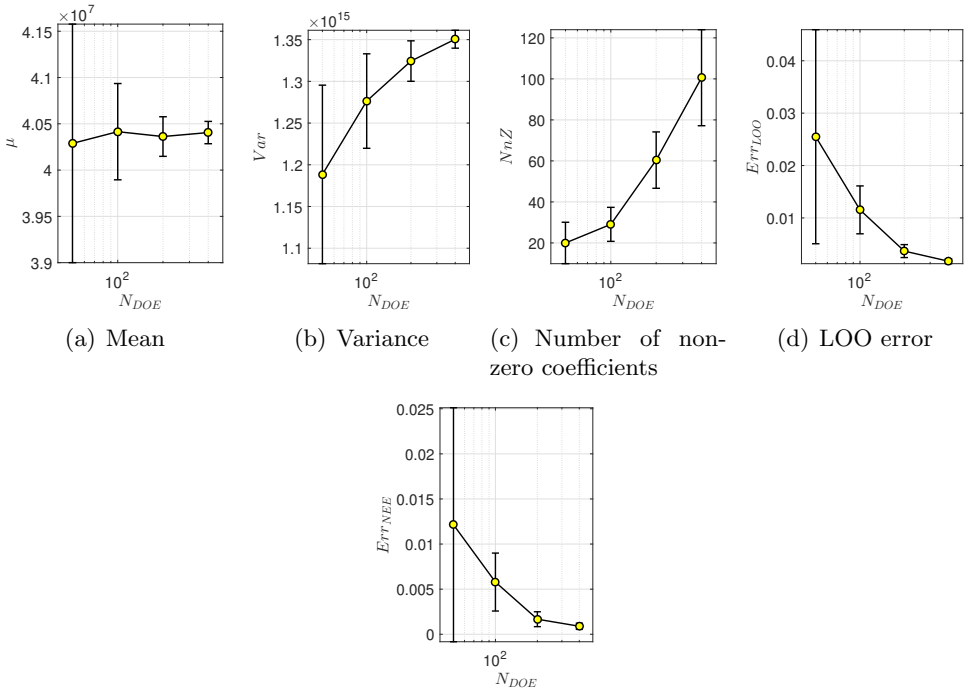

(a) Mean (b) Variance (c) Number of non-zero coefficients (d) LOO error

(e) NEE error

Figure 6: Example 1; Uncertainty quantification of PCE meta-model based on 100 replications of the analyses; N_{DOE} is variable; meta-modeling is based on Z

Evolution of the LS functions for different initial DOE values are shown in Figures 7(b) and 7(c). As seen, the smaller DOE values lead to dispersion of the curves. Evaluation of these curves at $Z = 0$ provides the failure probability of the model. The variation of P_f is shown in Figure 7(d), along with the reference one from MCS. Each curve is obtained by plotting a vertical line at $Z = 0$ (for example, the dashed blue line in Figures 7(b) and 7(c)), and compute the CDF of all the crossing points. Ideally, the CDFs from PCE should predict the crude MCS at their median (CDF = 0.5). In other words, they should cross the yellow point in Figure 7(d). Nearly all the PCE meta-models tend to underestimate the P_f (meaning that cumulative P_f curves resulted from PCE are un-symmetry with respect to crude MCS). The model based on 50 DOE points, predicts the P_f to be 12.0% (while the $P_f^{MCS} = 13.3\%$). Increasing the number of DOE points, makes the curves symmetry, and the median of P_f^{PCE} yields to P_f^{MCS}.

Next, it is important to quantify the relation between performance of the PCE meta-model and the failure probability. Since the current example yields to P_f of 13.3%, 21 other models are generated with different failure probabilities. This is possible by changing width of the base, and also the initial crack length at the dam-foundation interface. For each of 21 models, the failure probability is computed 50 times, each time using 1,000 samples. Therefore, a matrix of 50×21 is developed for $P_f^{Analytical}$ as seen in Figure 8(a). According to this plot, the failure probability varies from 30% to about 0.1% (with most of the cases categorized as small failure probability models).

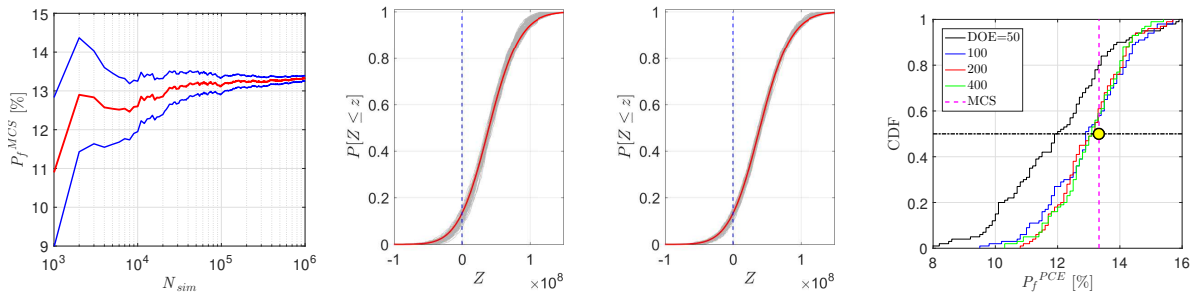

(a) Crude MCS (b) PCE; $N_{DOE} = 50$ (c) PCE; $N_{DOE} = 100$ (d) PCE; P_f

Figure 7: Example 1; Reliability assessment of PCE meta-model; N_{DOE} is variable; meta-modeling is based on P_f

The mean and standard deviation of failure probability is computed for each model based on analytical calculations. In addition, the PCE meta-model is used with different number of initial DOEs to estimate P_f. Finally, the ratio of mean and STD of the PCE meta-models with respect to the analytical one is plotted in Figures 8(b) and 8(c) as a function of $P_f^{Analytical}$ and N^{DOE}. As seen, the performance of the system degrades for smaller failure probabilities. For a system with $P_f = 10\%$, the PCE meta-models are 90-98% accurate (depending on the DOE size). This range becomes 70-85% for a system with only 0.5% probability of failure (i.e., only 5 failed simulations out of 1,000). This implies that a larger DOE needs to be used for the rare events. Finally, Figure 8(c) shows that the standard deviation of system is more stable for a larger DOE size, and it is not practically affected by P_f.

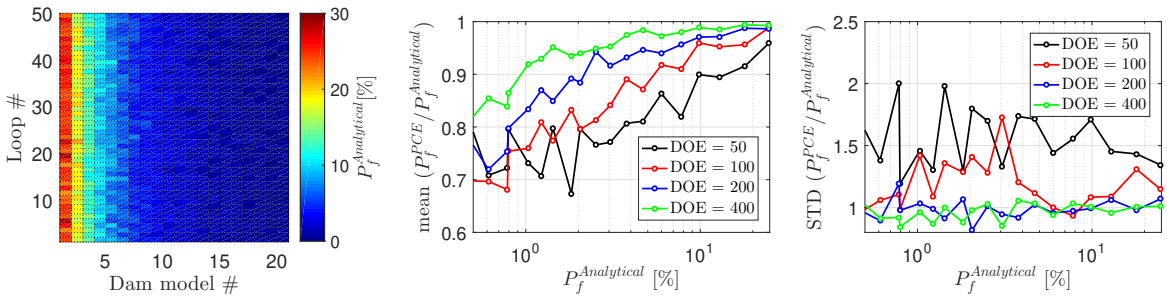

(a) Full FE results (b) mean; ratio of PCE to FEM (c) STD; ratio of PCE to FEM

Figure 8: Example 1; Performance of the PCE meta-model under uncertain P_f and variable N_{DOE}; meta-modeling is based on P_f

Sampling is the main issue in the material uncertainty quantification. In all the previous analyses, the LHS (Iman and Conover, 1982) was used for sampling. It is an efficient space filling sampling method which is categorized under pseudo-random sequences. These sequences are not truly random, because they are completely determined by an initial value, called the pseudo-random number generator's seed (Hariri-Ardebili and Pourkamali-Anaraki, 2019). Therefore, if two LHS-based (small) seeds are used for meta-modeling, they may lead

to slightly different results. The alternative solution is to adopt a quasi-random sequence. They are generated based on a completely deterministic low-discrepancy process and have no inherent statistical properties. Two famous sequences are Halton (Halton, 1964) (which is defined by bases of prime numbers. Each dimension requires a unique prime number as a base), and Sobol (Sobol', 1967) (which benefits the base of two to construct finer uniform partitions of the unit interval and then reordering the coordinates in each dimension. It looks almost like a grid in lower dimensions, but forms a lower discrepancy pattern at higher dimensions) (Hariri-Ardebili and Pourkamali-Anaraki, 2019).

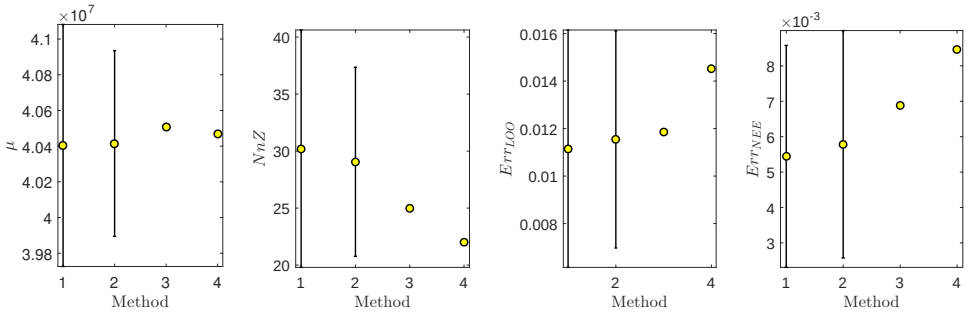

(a) Mean (b) Number of non-zero coefficients (c) LOO error (d) NEE error

Figure 9: Example 1; PCE meta-model; LAR technique; $N_{LHS} = 1,000$; $N_{sampling} = 100$; $q = 0.75$; methods: 1=MCS, 2=LHS, 3=Sobol, 4=Halton; meta-modeling is based on Z

Figure 9 illustrates the variation of the major parameters for a case with $q = 0.75$, $N_{sampling} = 1000$, and $N_{DOE} = 100$. Four sampling methods are compared, i.e. crude MCS, LHS, Sobol, and Halton. Since two latter methods are quasi-random techniques, they do not generate any dispersion in the statistical analyses. The predicted mean value from all four techniques is practically identical. The behavior of MCS and LHS is very close. For the small batch of DOE their variations are similar. On the other hand, Halton and Sobol show a bit different response. They both reduce the NnZ and increase the residual errors. Again, from practical point of view, one may prefer to use those low-discrepancy sequences because they do not generate a relatively large variation in the metrics. This may give extra confidence in decision-making.

4.2 Simplified Gravity Dam Finite Element Model

In this second example, a series of probabilistic seismic analyses are performed on a simplified model of gravity dam including epistemic uncertainties (due to lack of knowledge about exact material properties). A total of $N_{sim} = 1,000$ time history analyses are performed, and used as reference model. Results are extracted in terms of the displacement and stress (both principal and normal/shear) time histories for all the nodes, and elements. Among many QoIs, the horizontal crest displacement, and vertical stress at the heel are the most important ones, since they provide the global state of the dam.

Similar to the previous example, the first step is to provide a general overview of the predicted results and the expansion coefficients. They are shown in Figure 20 for different sizes of the initial DOEs ranging from 50 to 200. Y represents the displacement in mm. Again, the LAR method is used with q=0.75 in all cases. One major difference between Figures 20 and 5 (second row) is that in the latter one (i.e. with explicit LS) the degree of available (or contributing) expansion coefficients increase by the increase in N_{DOE}. This is not the case in the former one (i.e. implicit LS), and degree 3 and higher ones exist on all DOE sizes.

Again, a statistical method is used to quantify the meta-models with different DOE values, Figure 10. One hundred samples are taken for each N_{DOE}, and the mean and STD of different metrics are evaluated. Two QoIs are used (i.e. displacement and stress) to contrast suitability of various outputs during surrogating. The following observations can be drawn:

- Mean value is nearly stable after $N_{DOE} = 100$, Figure 10(a). The STD of its variation is also reduced for both displacement and stress QoIs. There is no meaningful difference between the two QoIs.
- Variance of the meta-model is increased by increasing the N_{DOE}, while its STD yields a small value, Figure 10(b). The rate of increase is lower for the stress response.
- Although not surprising, the mean and STD of the non-zero coefficients is also increased by N_{DOE}, Figure 10(c).
- Both the LOO and NEE residual errors decrease with increasing N_{DOE}, Figures 10(d) and 10(e). For smaller N_{DOE} values, the stress QoI leads to higher error; however, both the QoIs yield to nearly same value at $N_{DOE} = 400$, i.e. less than 1% error, which is more than sufficient for an engineering purpose.

So far, all the meta-models were based on scalar QoI at an index point (i.e. crest or heel). It is important to evaluate the sensitivity of the PCE meta-models to the location of the response. Figure 11 illustrates some of the metrics along the height, H, of the dam. Since displacement and stress response have similar trend, this figure focuses only on the displacement QoI.

Figures 11(a) to 11(d) provide the metrics for the case with $N_{DOE} = 50$ (as pilot case in this series). Observations can be summarized as follows:

- The mean value of the displacement increases with the height coordinate, Figure 11(a). This is consistent with the physics of the problem. STD is negligible compared to mean.
- According to Figure 11(b), the variance also increases by H. One can divide this curve into two linear parts: $H \in [0, 65]$ and $H \in [65, 103]$. The former belongs to the main body (which increases slowly), and the latter presents the slender neck area (with a sharp increase). STD increases continuously by height.

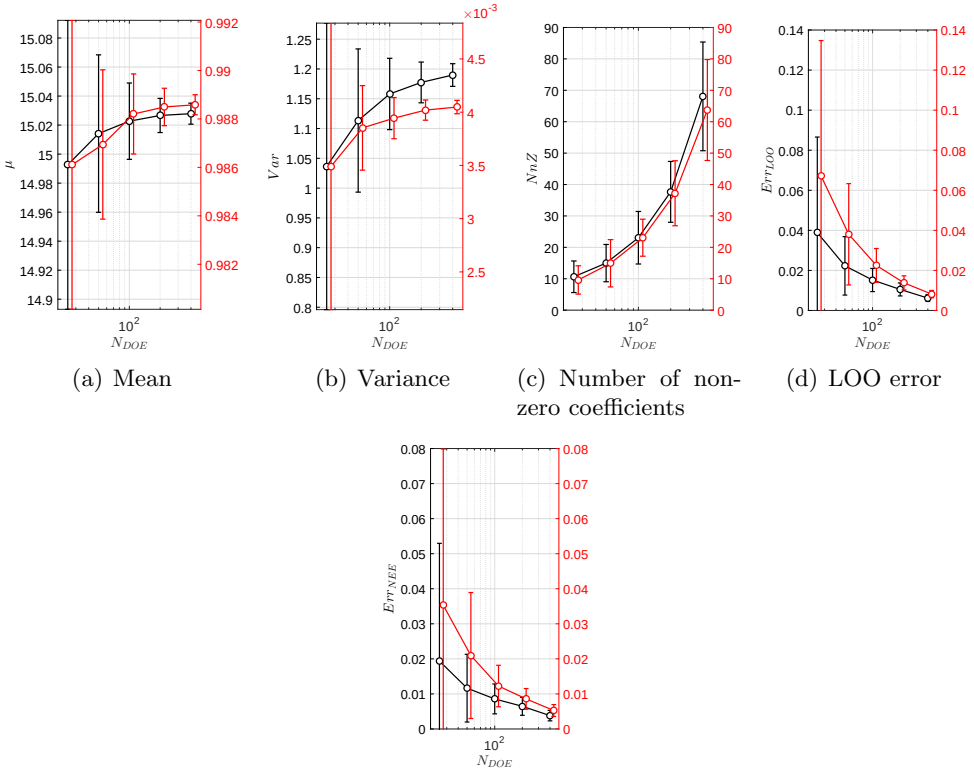

(a) Mean (b) Variance (c) Number of non-zero coefficients (d) LOO error

(e) NEE error

Figure 10: Example 2; Uncertainty quantification of PCE meta-model; N_{DOE} is variable; black line: crest displacement in [mm]; red line: heel vertical stress in [MPa]; Note: the red curves are shifted a bit right to avoid overlapping with black ones

- The LOO residual error is shown in Figure 11(c) (NEE is similar and thus is skipped). Again, it seems that the behavior of main body and neck is different. The Err_{LOO} increases up to height of 60-70 m, then it shows a reduction.
- Finally, Figure 11(d) shows that the number of non-zero expansion coefficients fluctuates between 14-19. There is a uniform pattern along the height.

Next, the impact of N_{DOE} is evaluated along the upstream face of dam. For μ and Var only the STD values are shown (as there is no meaningful change in mean). For Err_{LOO} and NnZ the mean value is plotted (as there are large changes). According to Figures 11(e) and 11(f), the STD_{μ} and STD_{Var} is reduced by increasing N_{DOE}. Transition from 100 to 200 samples is negligible (not shown here). Moreover, there is a jump from 25 to 50 samples in the $\text{mean}_{Err_{LOO}}$, Figure 11(g). Finally, the mean_{NnZ} is nearly uniform for different N_{DOE} values, Figure 11(h).

4.3 Coupled Arch Dam-Reservoir-Foundation Model

In this third example, the seismic response of an arch dam-foundation-reservoir coupled system is studied subjected to a three-component ground motion. Since this is a detailed time history analysis, the number of FE simulations are limited. The objective is to evaluate

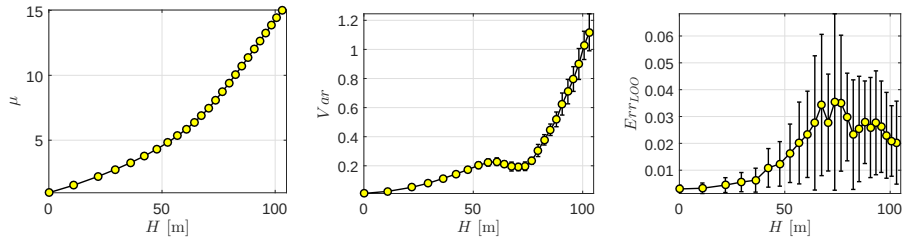

(a) Mean; $N_{DOE} = 50$ (b) Variance; $N_{DOE} = 50$ (c) LOO error; $N_{DOE} = 50$

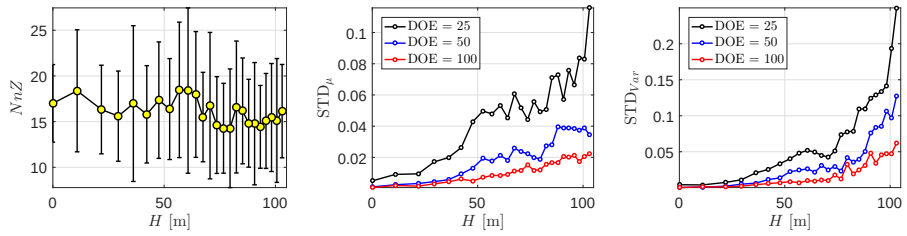

(d) Non-zero coefficients; $N_{DOE} = 50$ (e) Dispersion of mean (f) Dispersion of variance

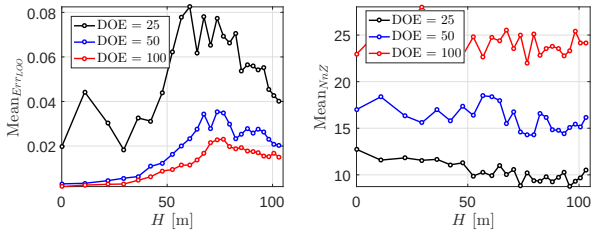

(g) Average of LOO error (h) Average of non-zero coefficients

Figure 11: Example 2; Variation of PCE metrics along the upstream face of the dam; N_{DOE} is fixed to 50 in the first row, and is variable for the second row; only crest displacement; Unit = [mm]

the applicability of the PCE even with small number of initial simulations. Results are extracted in terms of displacement and principal time histories for all the nodes and the elements. The following set of simulations are performed:

- LHS-based approach: several batches of 100, 50 and 25 simulations.
- Sobol and Halton samplings: two batches of 50 simulations for each.

Hereafter, the batch with 50 LHS points is assumed to be the pilot model. All others are evaluated with respect to this batch. Figure 21 provides a general overview of the predicted results (i.e. maximum absolute crest horizontal displacement as Y) and the expansion coefficients. All those four results are based on LHS with different initial samples. Again, LAR method is used with q=0.75 in all models. Differences of Figure 21 with respect to Figures 20 and 5 (second row) is that it includes only coefficients 1 to 20 for any sample size. Moreover, all those coefficients are non-zero and independent of initial N_{DOE}. Obviously, the meta-model with 25 samples has poor quality, while $N_{DOE} = 50$ is good for any practical application (The Err_{LOO} for the models with $N_{DOE} = 50$ is in the order of 10^{-3}, while it

is much bigger for $N_{DOE} = 25$).

Since the stress distribution in arch dams is the governing factor in safety assessment of these infra-structures, it is important to evaluate the capability of the PCE in prediction of spatial QoIs with the body. Figure 12 illustrates the main metrics for the first (S1) and third (S3) principal stresses within dam body. A coarse mesh is used for this academic example; however, one can simply refine the element size. Moreover, only half of the dam is shown due to its symmetry. The following conclusions can be drawn:

- For S1, the higher values of the mean are observed close to the base and also in the vicinity of the crest. However, for S3, the crest level next to abutment has the highest (absolute) mean stress value.
- In term of variance, moving upward (along the height) decreases the variance for S1. In the case of S3, the variance takes higher values at the bottom and crest, while it is minimum in mid-height.
- The residual errors have, in general, a uniform pattern within the body. There are some localized area in which the elements' error is higher than the neighboring ones. This is limited to one element at the base of dam for S1, and one element next to the abutment in S3.

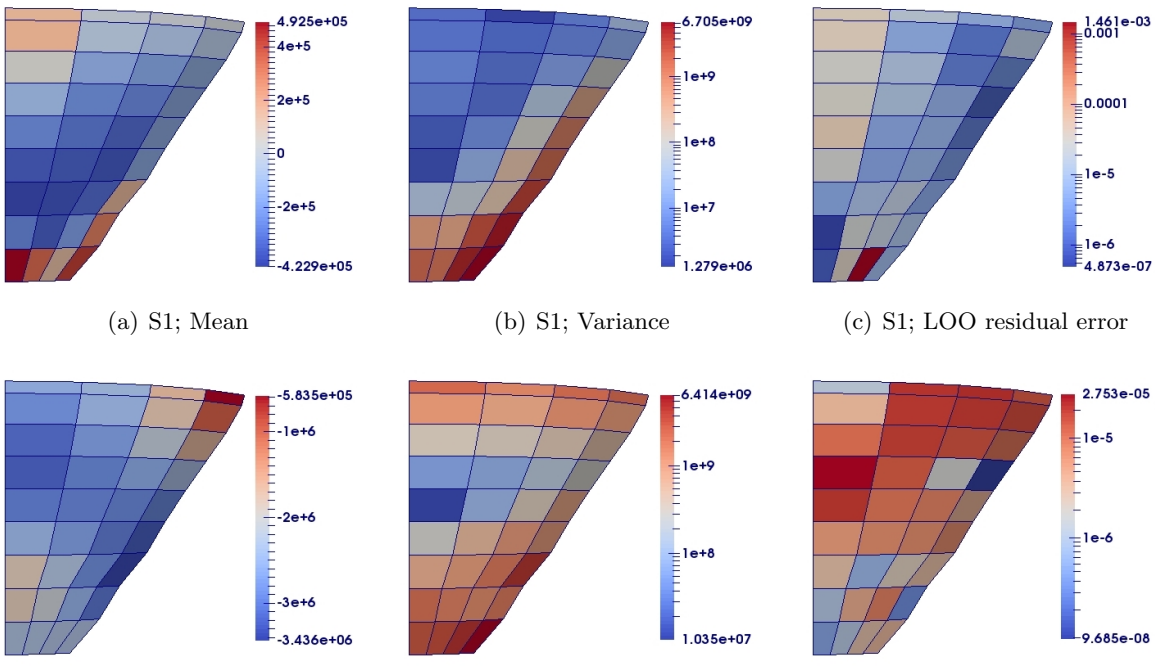

(a) S1; Mean (b) S1; Variance (c) S1; LOO residual error

(d) S3; Mean (e) S3; Variance (f) S3; LOO residual error

Figure 12: Example 3; Coupled arch dam; PCE meta-model; LHS-based $N_{DOE} = 50$; elemental principal stresses over dam body; Unit = [Pa]

Figure 12 only presented the state of the metrics qualitatively for LHS-based sampling with $N_{DOE} = 50$. Figure 13, indeed, expand this model for various initial sample sizes.

Moreover, in order to refine the search and meta-modeling, the nodal principal stresses (only S1 in this plot) is used instead of the previous elemental values (which are practically averaged over all connectivity nodes). The following observations can be reported:

- According to Figure 13(a), the μ value of different sample sizes are very close.
- Variation of variance, Figure 13(b), is pretty complex. Variation of the model with $N_{DOE} = 100$ is more uniform. In general, the variance of the model with $N_{DOE} = 25$ is higher.
- Variation of the LOO residual error along different nodes is nearly uniform, Figure 13(c). In general, decreasing the sample size, increases the error values.

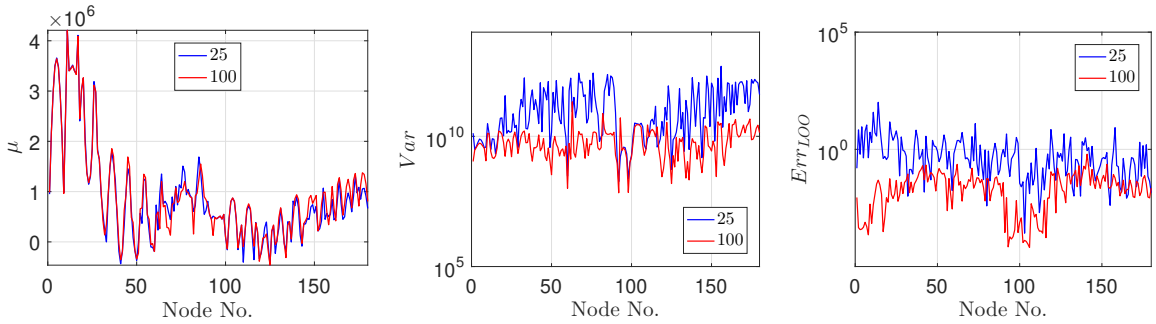

(a) Mean (b) Variance (c) Residual error LOO

Figure 13: Example 3; Coupled arch dam; PCE meta-model; LHS-based N_{DOE} is variable; nodal first principal stresses over dam body; Unit = [Pa]

Figure 14 compares different meta-models all with 50 initial DOE and different sampling techniques (i.e. LHS, Sobol and Halton). Ignoring the small changes, one may conclude that there is practically no differences among three techniques for this kind of problems.

Both the results in Figures 13 and 14 are based nodal S1. Similar conclusions were obtained for S3 (not shown here).

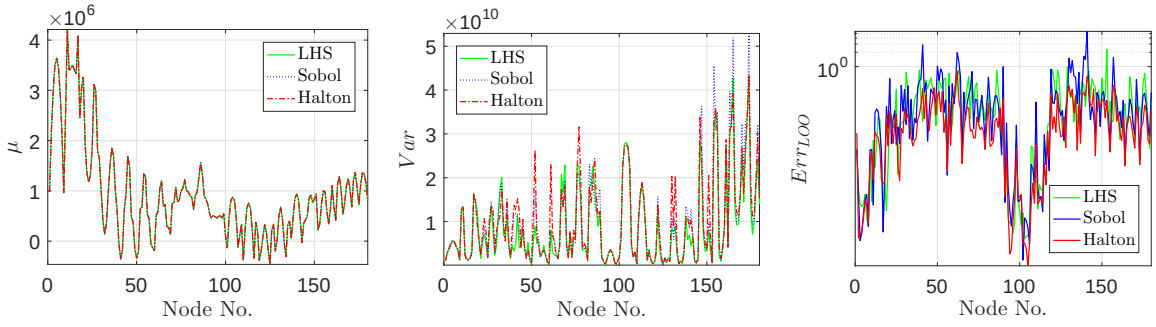

(a) Mean (b) Variance (c) Residual error LOO

Figure 14: Example 3; Coupled arch dam; PCE meta-model; different sampling techniques; $N_{DOE} = 50$; nodal first principal stresses over dam body; Unit = [Pa]

So far, all the results are based on a scalar value of the maximum/minimum non-concurrent stress values over the nodes/elements. Figure 15 explores the application of

the PCE-based meta-modeling on direct time history data. In the present paper, a response history is treated as a vector of many QoIs acting independent from each other. Since the duration of the applied ground motion is 40.0 s with the time step of 0.02 s, there exists 2,000 data points in any response history. To develop the meta-model for the time-dependent QoIs, a loop with 2,000 iterations is written around the core PCE function. The values of QoIs (i.e., displacements in Figure 15) are predicted at each iteration (which corresponds to a particular time instance). Once all the time increments are predicted, they are assembled again in a vector form to build the estimated response history.

The original FEM-based displacement time history (at the center of crest), and the PCE-based predicted one are shown in Figures 15(a) and 15(b), respectively. Qualitatively, the meta-modeling seems to be very good. Both the appearance of the time history and its peak values are preserved. Then, the results are plots next to each other and the time parameter is ignored, Figure 15(c). As seen, the individual QoIs at various time instance are very close to the equity line.

The mean and variance of the crest time history predicted by the PCE are shown in Figures 15(d) and 15(e), respectively. As expected, the general trend of μ is very similar to trajectory obtained for the mean value of the parameters. Moreover, the peak points of the variance correspond to the jumps in displacement time history. Finally, the LOO residual error is illustrated in Figure 15(f). It seems that the error fluctuates around 10^{-3} with the boundaries of 10^{-5} and 10^{-1}. Higher error values correspond to the higher displacement responses.

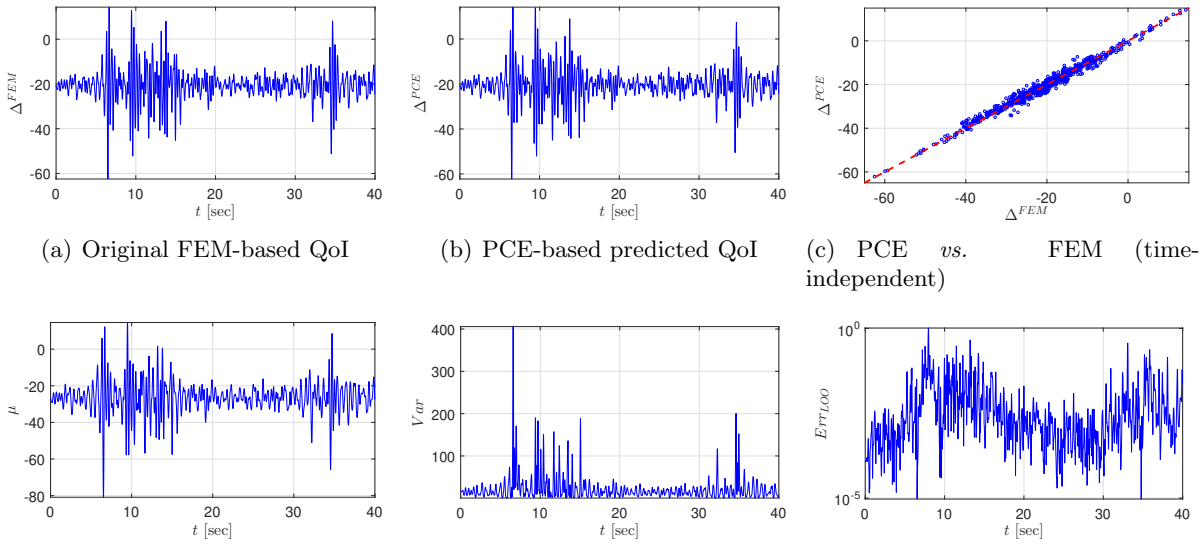

(a) Original FEM-based QoI (b) PCE-based predicted QoI (c) PCE *vs.* FEM (time-independent)

(d) Mean (e) Variance (f) LOO error

Figure 15: Example 3; Coupled arch dam; PCE meta-model; LHS-based $N_{DOE} = 50$; time history of crest displacement; Unit = [mm]

Finally, the PCE-based meta-model is compared with a neural network based model. A classical NN is adopted with the architecture of Figure 16(a). It contains a scaling layer

(gray circles), a neural network (dark-blue circles are perceptron neurons), and an un-scaling layer (red circle). The number of input parameters is three (according to Table 3), and the output is maximum crest displacement (obtained from time history analyses). Two neural networks are trained with 50 and 100 initial design of experiments. On the other hand, the same DOEs are used in the PCE-based meta-model. Finally, the predicted displacements are compared with the FEM-based ones for both the PCE and NN meta-models.

Although there are different scalar metrics to compare the models (e.g., coefficient of determination, root mean square error, mean absolute error, etc.), the cumulative error percentage is used in this paper. It provides the detailed variation of the error parameter for the meta-models, Figures 16(b) and 16(c). Although both meta-models have satisfactory performance for the practical/engineering purposes, the PCE is clearly superior to NN. The error percentage from PCE-based meta-model varies between [-0.5, +0.5]%, while the one from NN varies between [-4.0, +1.5]% (with a large lower tail). Again, detailed comparison of PCE with other surrogate models (and not specifically NN) is beyond the scope of this paper. However, Figure 16 was provided only for the illustrative purposes.

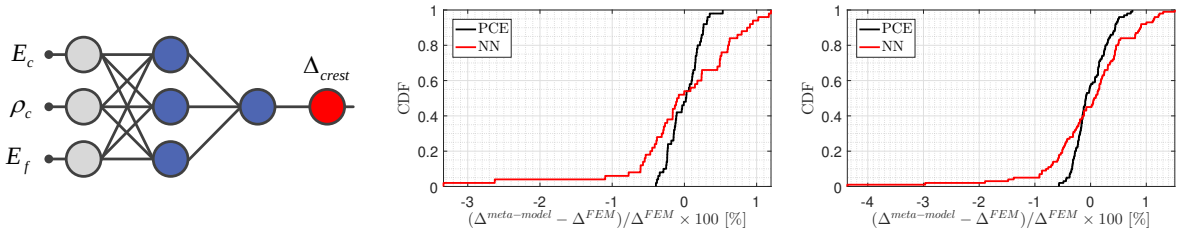

(a) Neural network architecture (b) $N_{DOE} = 50$ (c) $N_{DOE} = 100$

Figure 16: Example 3; Coupled arch dam; PCE *vs.* NN meta-models; variable N_{DOE}; maximum crest displacement in [mm]

4.4 Layered Arch Dams Vibration Characteristics

This example deals with modal analysis of an arch dam with different layers of concrete and modulus of elasticity. QoIs, in this section, are: 1) vibration frequencies, 2) participation factors, and 3) effective masses. Since the dam is a shell-type 3D continuum structure, three translations and three rotational quantities can be extracted for each mode.

Using the LHS techniques, 1,000 samples with random modulus of elasticity are generated, and the first 30 vibration modes are extracted, Figure 17(a). Evolution of the cumulative normalized effective masses in translational and rotational directions are also shown in Figures 17(b) and 17(c). The cumulative normalized masses sum up to one for the first 30 frequencies, and thus, one may truncate the higher order modes. There are two important points:

- Correlation of different frequencies, Figure 17(d). As seen, there is a certain correlation

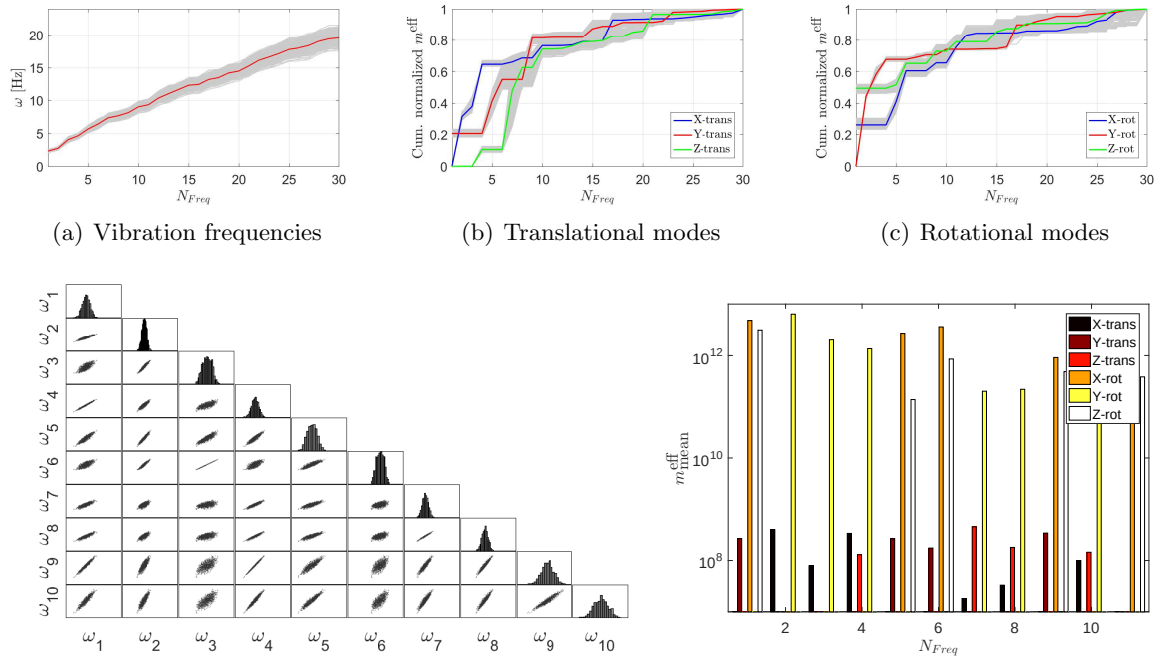

(a) Vibration frequencies (b) Translational modes (c) Rotational modes

(d) Dependency of modes (e) Effective modes

Figure 17: Example 4; Layered arch dam; general characteristics of the vibration analysis obtained from the 1,000 points of the DOE

among different modes, and the meta-model should preserve this dependency. For example, there is a strong correlation between (ω_1, ω_2) and (ω_1, ω_4), while it is weak between (ω_1, ω_3). It means that the fourth frequency is always increased with an increase in the first one; and this variation is independent of the material randomness in six dam layers. On the other hand, the relative variation of the first and third frequencies highly depends on the material properties.

One should note that for an elastic system with homogeneous material, the correlation between different modes is always full (i.e., the correlation coefficient is unit) during a probabilistic analysis. Increasing the inhomogeneity (in the form of orthotropic layered material or heterogeneous ones), reduces the correlation coefficient between different modes (Hariri-Ardebili et al., 2019) for any random field simulation. In order to develop an appropriate meta-model, not only the frequency values but also their relative correlation should be incorporated in PCE-based algorithm.

- Effective direction in each mode, Figure 17(e). Any classical modal analysis yields different effective masses in six directions for each mode. However, it does not mean that a particular mode is important in all directions. The relative effective mass can be used to distinguish the effective direction in each mode. Figure 17(e) shows the mean (over the 1,000 samples) effective mass for the first 11 modes. It is bounded to 10^7 to 10^{13} to focus on the effective modes. For example, Y-trans, X-rot and Z-rot are three (relatively) important directions for mode one. For the second mode, X-trans

and Y-rot are important, and so on. As a general observation, there are only two or three active directions in each mode. The PCE meta-model will focus on these effective modes in each direction and will skip the others.

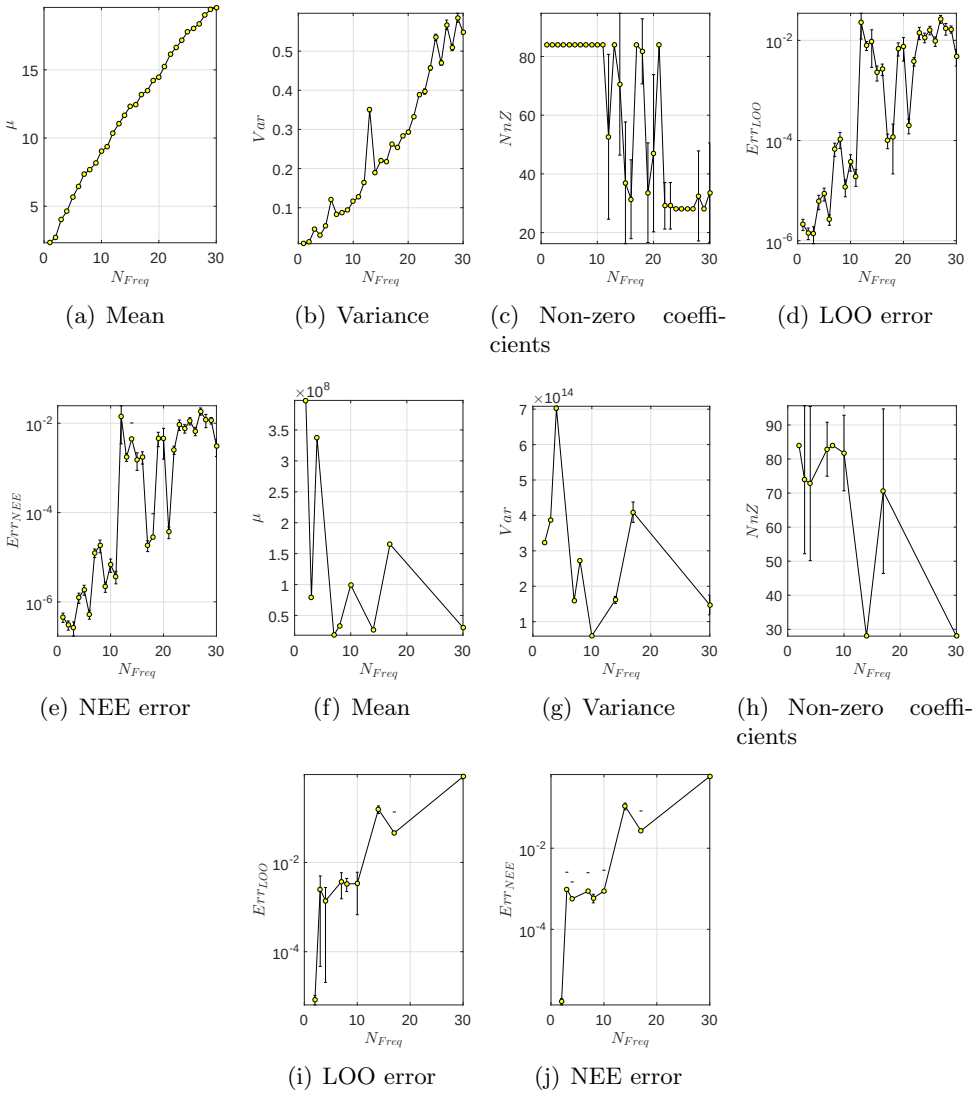

(a) Mean (b) Variance (c) Non-zero coefficients (d) LOO error

(e) NEE error (f) Mean (g) Variance (h) Non-zero coefficients

(i) LOO error (j) NEE error

Figure 18: Example 4; Layered arch dam; $N_{LHS} = 1000$; $N_{DOE} = 200$; two QoIs

A batch with 200 initial DOEs is selected using LHS technique, and considered to be the pilot model. Figures 22 and 23 provides a general overview of the predicted results (i.e. frequencies in the first 15 modes as Y) and the expansion coefficients, respectively. The quality of prediction is very good for the first 11 modes. They have the expansion coefficients up to 3rd degree. Predicted results for modes 12 to 15 is fairly good, and only the 2nd degree coefficients exist. Similar to the previous examples, the LAR method is used with q=0.75 in all meta-models. The major difference of Figure 23 compared to Figures 21, 20 and 5 (second row) is that nearly all the coefficients are non-zero, and there is a uniform and decaying nature in $log(|y_\alpha|) - \alpha$ plot. This means that the resulting PCE are not really sparse for eigenfrequency analysis.

Figure 18 summarizes the results of probabilistic PCE meta-model for different QoIs and directions. Two sets of results are studied:

- General frequency response, Figures 18(a) to 18(e).
  - The mean and variance both increase as a function of frequency. The mean is quite uniform, while there are some nonlinear variations for the variance.
  - The NnZ is constant and equal to 80 for the first 11 modes (without any dispersion).
  - Both the residual errors have similar and increasing trend, with relatively large variation and small dispersion.
- Effective mass in X direction, Figures 18(f) to 18(j).
  - These results represent all six directions. For other translational and rotational directions, one may drive similar conclusions.
  - The results are shown only for 9 effective modes.
  - There is no general observation for mean and variance.
  - In general, smaller frequencies have higher NnZ.
  - In general, both the residual errors are increased by frequency.

Finally, the impact of the DOE size on the quality of meta-model is investigated in Figure 19. The following observations can be drawn:

- The mean (not shown here) and variance of different sample sizes are practically identical.
- Increasing the DOE size, increases the number of NnZ coefficient.
- Both the residual errors have an increasing trend. Increasing the DOE size, decreases the residual errors.

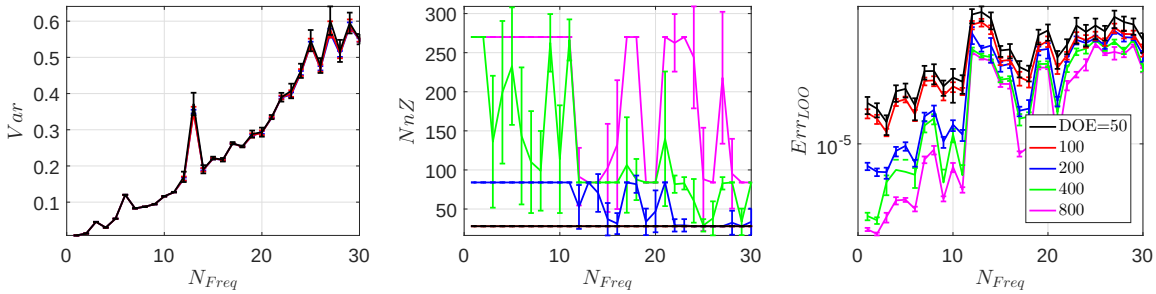

(a) Variance (b) Non-zero coefficients (c) LOO error

Figure 19: Example 4; Layered arch dam; $N_{LHS} = 1000$; N_{DOE} is variable; only frequency response

5 Summary

Concrete dams are part of the critical infrastructural systems which provide drinking water, and can be used for irrigation and/or generate hydro-power electricity. Yet, dams are aging and many of them were built at the time with limited information about the natural hazards. Therefore, periodic safety assessment of dams is an essential task to keep the integrity of the national-wide infrastructural systems. Risk-based safety assessment is an approved method by International Commission on Large Dams, and many of other national legislation. However, large portion of the current practice in dam engineering is based on the deterministic analysis with engineering judgment, or limited probabilistic analyses. Despite the fact that there are many uncertainties associated with a dam analysis, the complexity of the simulations and the computational burden for the probabilistic analyses are the major inhibitors for a comprehensive uncertainty quantification.

This paper proposed the application of Polynomial Chaos Expansion as an effective method in uncertainty quantification of complex infra-structures. Four examples of concrete dams with different complexities were investigated: 1) analytical model of a gravity dam, 2) simplified finite element analysis of a gravity dam, 3) detailed coupled analysis of an arch dam-foundation-reservoir system, and 4) frequency analysis of an arch dam with stage construction. These case studies were selected because they had different features and complexities and seek different QoIs related to the concrete dam safety assessment.

In all examples, a large initial dataset was developed (either from analytical solutions or the finite element analyses), and the ability of PCE in response prediction was evaluated with a very small portion of those data. All the detailed results including the comparison of 1) different sample sizes, 2) response parameters (i.e. QoI), 3) statistical parameters (e.g. mean, variance, error), 4) sampling methods (e.g. LHS, Halton, Sobol), and 5) location-based response values (i.e. spatial variability) can be found in the paper. There are not repeated here again. Overall, it is found that PCE can develop a meta-model with a very limited number of initial simulations and reduce the computational time considerably. Even the sample size with 5% of the initial dataset provides acceptable (engineering) results. Intuitively, by increasing the sample size the prediction error yields to zero. Findings of this research propose the application of PCE as a useful technique in uncertainty quantification of dam engineering problems with different material models, seismic ground motions, frequency analysis, heterogeneity, etc. The application is straightforward, and can be adopted easily by the practitioners.

Acknowledgments

The first author would like to express his sincere appreciation to his former advisor (and current mentor), Professor Victor E. Saouma at the University of Colorado Boulder for his

enthusiastic guidance and advice. The authors would also like to thank the reviewers for their helpful and constructive comments that greatly contributed to improving the final version of the paper.

References

F. Salazar, R. Morán, M. Á. Toledo, E. Oñate, Data-based models for the prediction of dam behaviour: A review and some methodological considerations, Archives of Computational Methods in Engineering (2015) 1–21.

M. A. Hariri-Ardebili, Risk, reliability, resilience (r3) and beyond in dam engineering: A state-of-the-art review, International journal of disaster risk reduction 31 (2018) 806–831.

J.-y. Chen, Q. Xu, J. Li, S.-l. Fan, Improved response surface method for anti-slide reliability analysis of gravity dam based on weighted regression, Journal of Zhejiang University-SCIENCE A 11 (2010) 432–439.

I. Karimi, N. Khaji, M. Ahmadi, M. Mirzayee, System identification of concrete gravity dams using artificial neural networks based on a hybrid finite element–boundary element approach, Engineering structures 32 (2010) 3583–3591.

S.-l. Fan, J.-y. Chen, J. Li, F. Wu-qiang, Roller compacted concrete gravity dams reliability analysis based on response surface approach, in: Earth and Space 2010: Engineering, Science, Construction, and Operations in Challenging Environments, 2010, pp. 3355–3367.

C. Gu, B. Li, G. Xu, H. Yu, Back analysis of mechanical parameters of roller compacted concrete dam, Science China Technological Sciences 53 (2010) 848–853.

A. Gaspar, F. Lopez-Caballero, A. Modaressi-Farahmand-Razavi, A. Gomes-Correia, Methodology for a probabilistic analysis of an rcc gravity dam construction. modelling of temperature, hydration degree and ageing degree fields, Engineering Structures 65 (2014) 99–110.

L. Cheng, J. Yang, D. Zheng, B. Li, J. Ren, The health monitoring method of concrete dams based on ambient vibration testing and kernel principle analysis, Shock and Vibration 2015 (2015).

H. Su, Z. Wen, S. Zhang, S. Tian, Method for choosing the optimal resource in back-analysis for multiple material parameters of a dam and its foundation, Journal of Computing in Civil Engineering 30 (2016).

M. Rezaiee-Pajand, F. H. Tavakoli, Crack detection in concrete gravity dams using a genetic algorithm, Proceedings of the Institution of Civil Engineers-Structures and Buildings 168 (2015) 192–209.

X. Cao, C. Gu, E. Zhao, Uncertainty instability risk analysis of high concrete arch dam abutments, Mathematical Problems in Engineering 2017 (2017).

M. A. Hariri-Ardebili, MCS-based response surface metamodels and optimal design of experiments for gravity dams, Structure and Infrastructure Engineering 14 (2018) 1641–1663.

M. A. Hariri-Ardebili, F. Pourkamali-Anaraki, Support vector machine based reliability analysis of concrete dams, Soil Dynamics and Earthquake Engineering 104 (2018a) 276–295.

M. A. Hariri-Ardebili, F. Pourkamali-Anaraki, Simplified reliability analysis of multi hazard risk in gravity dams via machine learning techniques, Archives of Civil and Mechanical Engineering 18 (2018b) 592–610.

M. A. Hariri-Ardebili, J. Xu, Efficient seismic reliability analysis of large-scale coupled systems including epistemic and aleatory uncertainties, Soil Dynamics and Earthquake Engineering 116 (2019) 761–773.

M. Hariri-Ardebili, F. Pourkamali-Anaraki, Matrix completion for cost reduction in finite element simulations under hybrid uncertainties, Applied Mathematical Modelling 69 (2019) 164–180.

R. Ghanem, G. Saad, A. Doostan, Efficient solution of stochastic systems: application to the embankment dam problem, Structural safety 29 (2007) 238–251.

X. Guo, D. Dias, C. Carvajal, L. Peyras, P. Breul, Reliability analysis of embankment dam sliding stability using the sparse polynomial chaos expansion, Engineering Structures 174 (2018) 295–307.

A. De Falco, M. Mori, G. Sevieri, Bayesian updating of existing concrete gravity dams model parameters using static measurements, in: 6th European Conference on Computational Mechanics (ECCM 6) - 7th European Conference on Computational Fluid Dynamics (ECFD 7), International Center for Numerical Methods in Engineering (CIMNE), Glasgow, UK, 2018, pp. 2245–2256.

M. A. Hariri-Ardebili, V. E. Saouma, Seismic fragility analysis of concrete dams: A state-of-the-art review, Engineering Structures 128 (2016) 374–399.

M. A. Hariri-Ardebili, S. M. Seyed-Kolbadi, V. E. Saouma, J. W. Salamon, L. K. Nuss, Anatomy of the vibration characteristics in old arch dams by random field theory, Engineering Structures 179 (2019) 460–475.

R. G. Ghanem, P. D. Spanos, Stochastic finite elements: a spectral approach, Courier Corporation, 2003.

B. Sudret, Global sensitivity analysis using polynomial chaos expansions, Reliability Engineering & System Safety 93 (2008) 964–979.

D. Xiu, G. E. Karniadakis, The wiener–askey polynomial chaos for stochastic differential equations, SIAM journal on scientific computing 24 (2002) 619–644.

N. Fajraoui, S. Marelli, B. Sudret, Sequential design of experiment for sparse polynomial chaos expansions, SIAM/ASA Journal on Uncertainty Quantification 5 (2017) 1061–1085.

G. Blatman, B. Sudret, Adaptive sparse polynomial chaos expansion based on least angle regression, Journal of Computational Physics 230 (2011) 2345–2367.

R. G. Ghanem, P. D. Spanos, Stochastic finite element method: Response statistics, in: Stochastic finite elements: a spectral approach, Springer, 1991, pp. 101–119.

M. Cavazzuti, Optimization methods: from theory to design scientific and technological aspects in mechanics, Springer Science & Business Media, 2012.

M. Berveiller, B. Sudret, M. Lemaire, Stochastic finite element: a non intrusive approach by regression, European Journal of Computational Mechanics/Revue Européenne de Mécanique Numérique 15 (2006) 81–92.

B. Efron, T. Hastie, I. Johnstone, R. Tibshirani, et al., Least angle regression, The Annals of statistics 32 (2004) 407–499.

S. Marelli, B. Sudret, Report UQLab-V0.9-104: UQLab user manual–Polynomial chaos expansions, Technical Report, Chair of Risk, Safety & Uncertainty Quantification, ETH Zürich, 0.9-104 edition, 2015.

G. Blatman, B. Sudret, An adaptive algorithm to build up sparse polynomial chaos expansions for stochastic finite element analysis, Probabilistic Engineering Mechanics 25 (2010) 183–197.

J. Friedman, T. Hastie, R. Tibshirani, The elements of statistical learning, volume 1, Springer series in statistics New York, 2001.

MATLAB, version 9.1 (R2016b), The MathWorks Inc., Natick, Massachusetts, 2016.

G. Fenves, A. Chopra, EAGD-84: A computer program for earthquake analysis of concrete gravity dams, University of California, Earthquake Engineering Research Center, 1984.

PEER, Ground motion database, `http://ngawest2.berkeley.edu/`, 2017. Last viewed June 2017.

M. McKay, R. Beckman, W. Conover, A comparison of three methods for selecting values of input variables in the analysis of output from a computer code, Technometrics 21 (1979) 239–245.

A. Olsson, G. Sandberg, Latin hypercube sampling for stochastic finite element analysis, Journal of Engineering Mechanics 128 (2002) 121–125.

M. Hariri-Ardebili, P. Boodagh, Taguchi design-based seismic reliability analysis of geostructures, Georisk: Assessment and Management of Risk for Engineered Systems and Geohazards (2018) 1–19.

C.-Y. Liaw, A. K. Chopra, Dynamics of towers surrounded by water, Earthquake Engineering & Structural Dynamics 3 (1974) 33–49.

N. Bouaanani, F. Y. Lu, Assessment of potential-based fluid finite elements for seismic analysis of dam–reservoir systems, Computers & Structures 87 (2009) 206–224.

H. Mirzabozorg, M. Varmazyari, M. Ghaemian, Dam-reservoir-massed foundation system and travelling wave along reservoir bottom, Soil Dynamics and Earthquake Engineering 30 (2010) 746–756.

M. A. Hariri-Ardebili, M. R. Kianoush, Integrative seismic safety evaluation of a high concrete arch dam, Soil Dynamics and Earthquake Engineering 67 (2014) 85–101.

Saouma, V., Numerical Modeling of AAR, CRC Press, 2014.

B. Sudret, Uncertainty propagation and sensitivity analysis in mechanical models–contributions to structural reliability and stochastic spectral methods, Habilitationa diriger des recherches, Université Blaise Pascal, Clermont-Ferrand, France (2007) 18.

S. Marelli, B. Sudret, Uqlab: A framework for uncertainty quantification in matlab, in: Vulnerability, Uncertainty, and Risk: Quantification, Mitigation, and Management, 2014, pp. 2554–2563.

R. Iman, W. Conover, A distribution-free approach to inducing rank correlation among input variables, Communications in Statistics-Simulation and Computation 11 (1982) 311–334.

J. H. Halton, Algorithm 247: Radical-inverse quasi-random point sequence, Communications of the ACM 7 (1964) 701–702.

I. M. Sobol', On the distribution of points in a cube and the approximate evaluation of integrals, Zhurnal Vychislitel'noi Matematiki i Matematicheskoi Fiziki 7 (1967) 784–802.

A. PCE-based Meta-model for Example 2

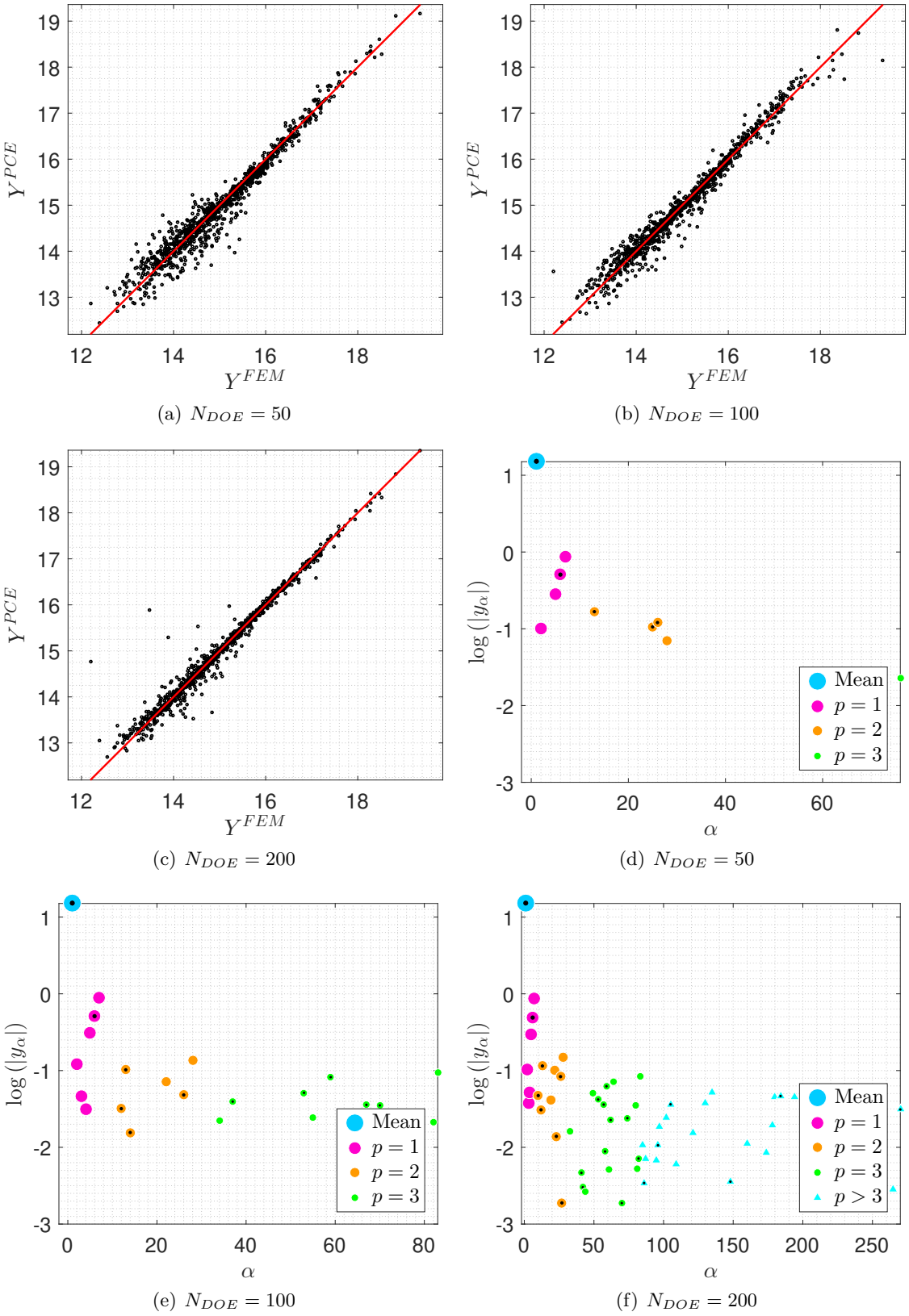

(a) $N_{DOE} = 50$ (b) $N_{DOE} = 100$

(c) $N_{DOE} = 200$ (d) $N_{DOE} = 50$

(e) $N_{DOE} = 100$ (f) $N_{DOE} = 200$

Figure 20: Example 2; Reference model; PCE meta-model; LAR technique; $N_{LHS} = 1000$; N_{DOE} is variable; only for crest displacement

B. PCE-based Meta-model for Example 3

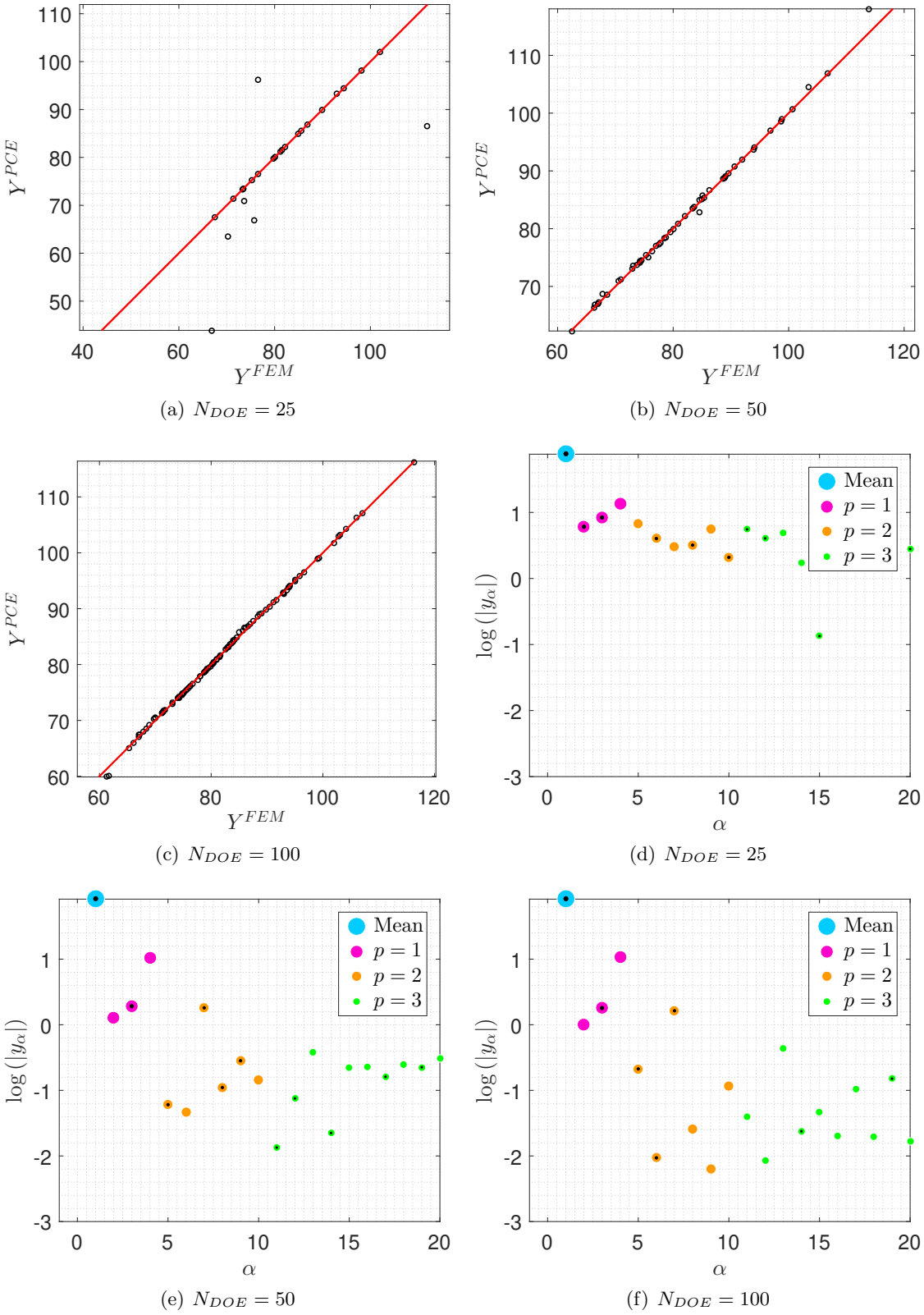

(a) $N_{DOE} = 25$ (b) $N_{DOE} = 50$

(c) $N_{DOE} = 100$ (d) $N_{DOE} = 25$

(e) $N_{DOE} = 50$ (f) $N_{DOE} = 100$

Figure 21: Example 3; Coupled arch dam; PCE meta-model; LAR technique; N_{DOE} is variable; maximum absolute crest displacement

C. PCE-based Meta-model for Example 4

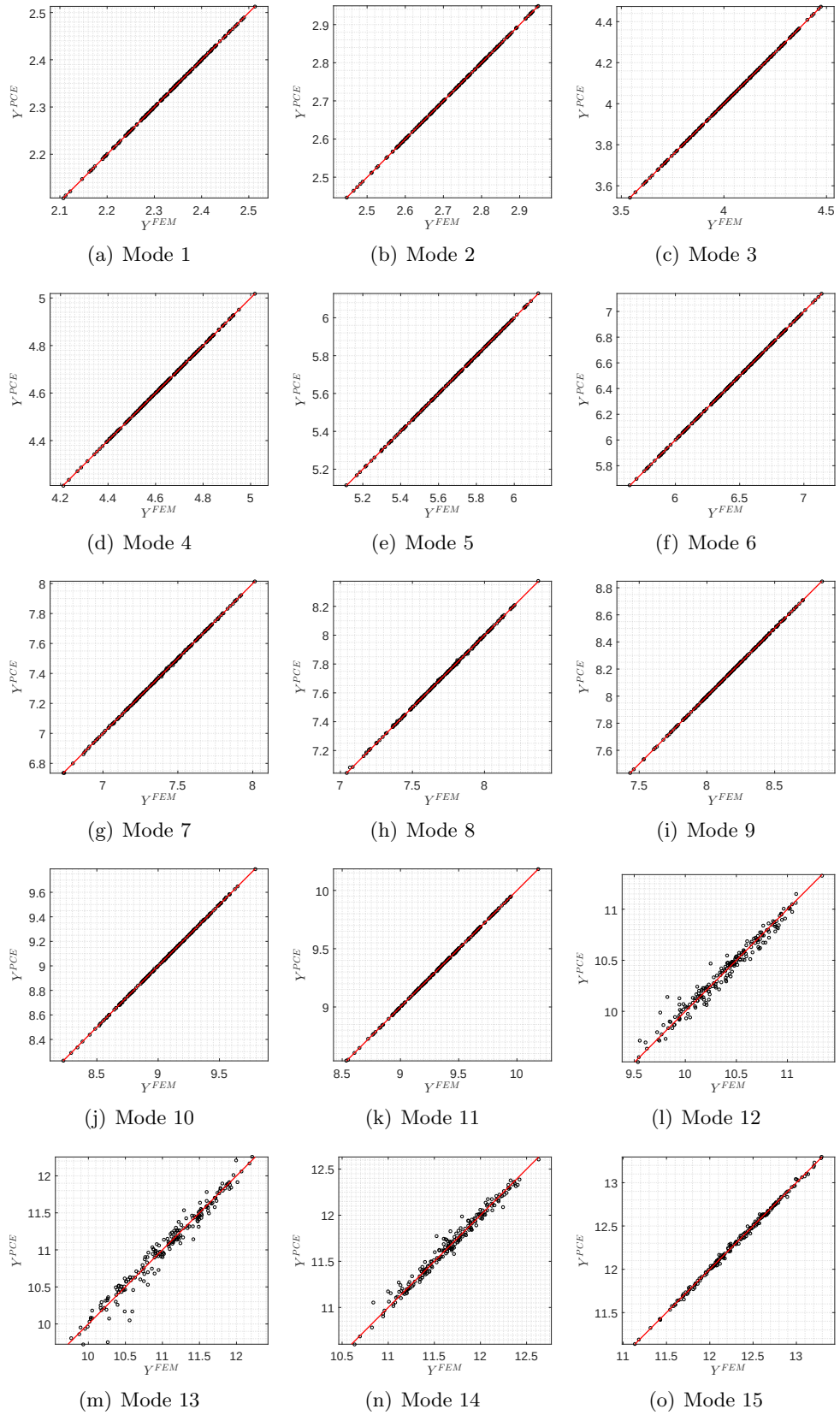

(a) Mode 1 (b) Mode 2 (c) Mode 3

(d) Mode 4 (e) Mode 5 (f) Mode 6

(g) Mode 7 (h) Mode 8 (i) Mode 9

(j) Mode 10 (k) Mode 11 (l) Mode 12

(m) Mode 13 (n) Mode 14 (o) Mode 15

Figure 22: Example 4; Layered arch dam; PCE meta-model; LAR technique; $N_{DOE} = 200$; quality of frequency prediction

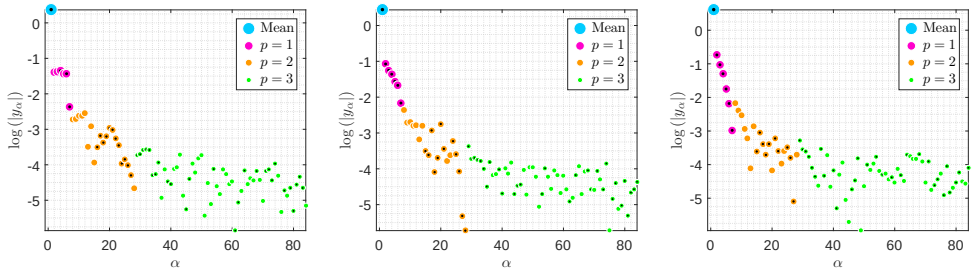

(a) Mode 1 (b) Mode 2 (c) Mode 3

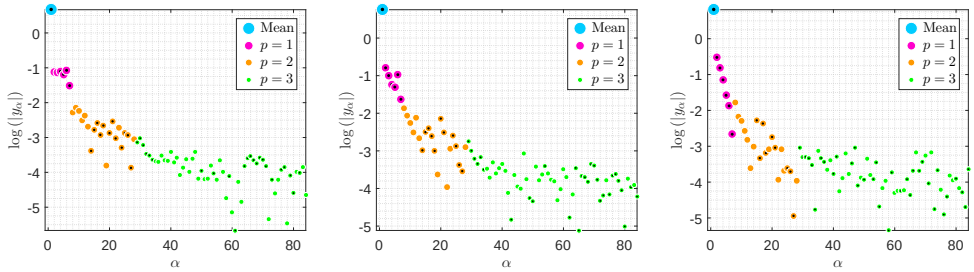

(d) Mode 4 (e) Mode 5 (f) Mode 6

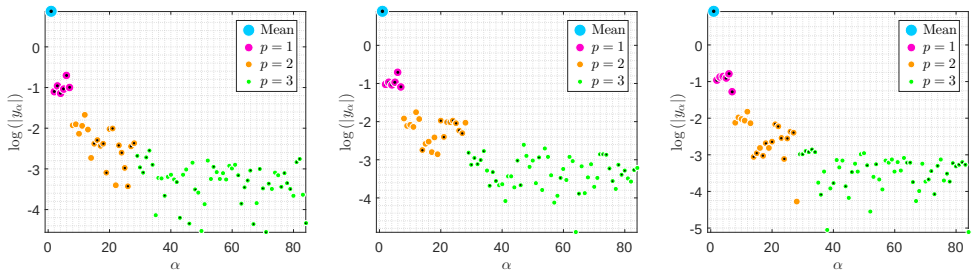

(g) Mode 7 (h) Mode 8 (i) Mode 9

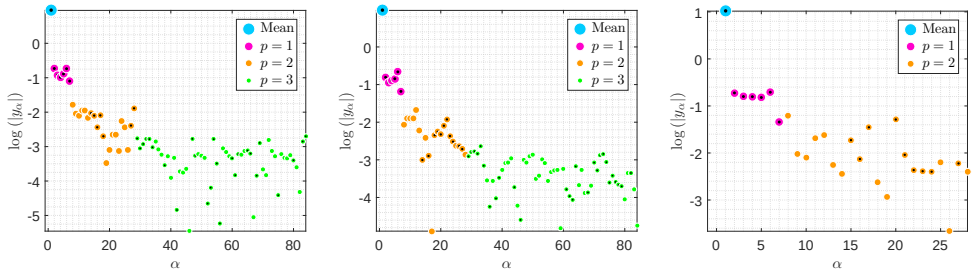

(j) Mode 10 (k) Mode 11 (l) Mode 12

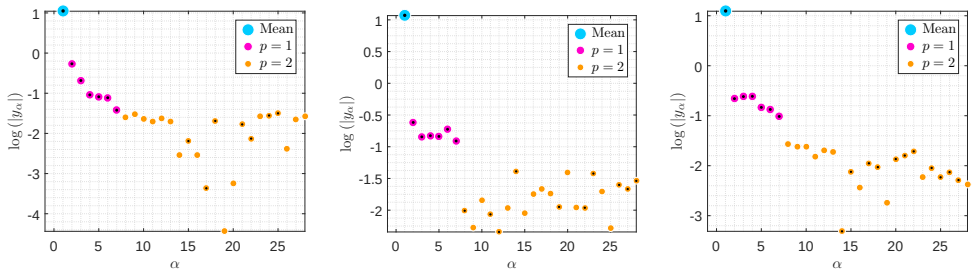

(m) Mode 13 (n) Mode 14 (o) Mode 15

Figure 23: Example 4; Layered arch dam; PCE meta-model; LAR technique; $N_{DOE} = 200$; expansion coefficients